

Motility and rotation of multiple-time-scale microswimmers in linear background flows

Eamonn A. Gaffney, Kenta Ishimoto on and Benjamin J. Walker on a Benjamin J. Walker

Corresponding author: Benjamin J. Walker, benjamin.walker@ucl.ac.uk

(Received 2 April 2025; revised 23 September 2025; accepted 28 September 2025)

Microswimming cells and robots exhibit diverse behaviours due to both their swimming and their environment. One key environmental feature is the presence of a background flow. While the influences of select flows, particularly steady shear flows, have been extensively investigated, these only represent special cases. Here, we examine inertialess swimmers in more general flows, specifically general linear planar flows that may possess rapid oscillations, and impose weak symmetry constraints on the swimmer (ensuring planarity, for instance). We focus on swimmers that are inefficient, in that the time scales of their movement are well separated from those associated with their motility-driving deformation. Exploiting this separation of scales in a multiple-time-scale analysis, we find that the behaviour of the swimmer is dictated by two effective parameter groupings, excluding mathematically precise edge cases. These systematically derived parameters measure balances between angular velocity and the rate of strain of the background flow. Remarkably, one parameter governs the orientational dynamics, whilst the other completely captures translational motion. Further, we find that the long-time translational dynamics is solely determined by properties of the flow, independent of the details of the swimmer. This illustrates the limited extent to which, and how, microswimmers may control their behaviours in planar linear flows.

Key words: low-Reynolds-number flows, active matter, micro-organism dynamics

1. Introduction

Microswimming cells, together with robotic swimmers at low Reynolds number, exhibit a myriad of behaviours and characteristics, in part due to the complexity of their actuation

© The Author(s), 2025. Published by Cambridge University Press. This is an Open Access article, distributed under the terms of the Creative Commons Attribution licence (https://creativecommons.org/licenses/by/4.0/), which permits unrestricted re-use, distribution and reproduction, provided the original article is properly cited.

¹Wolfson Centre for Mathematical Biology, Mathematical Institute, University of Oxford, Oxford OX2 6GG, UK

²Department of Mathematics, Kyoto University, Kyoto 606-8502, Japan

³Department of Mathematics, University College London, London WC1H 0AY, UK

and in part due to the diversity of their surrounding fluid environment (Lauga & Powers 2009; Gaffney et al. 2011; Elgeti, Winkler & Gompper 2015; Goldstein 2015; Huang et al. 2016; Diaz et al. 2021). A common feature of the microswimming environment is the presence of a background flow, which can influence microswimming in diverse ways. For instance, flows can induce guidance cues for cell navigation, often referred to as rheotaxis. Examples include sperm motility (Miki & Clapham 2013) and the behaviour of swimmers in microdevices, including algae such as *Chlamydomonas reinhardtii* (Omori et al. 2022) and bacteria such as Escherichia coli (Hill et al. 2007). Furthermore, investigations of the impact of a background flow are pertinent to the guidance of sperm cells in the female reproductive tract (Kolle et al. 2009; Miki & Clapham 2013; Kantsler et al. 2014), the design and control of microrobotic swimmers (Nelson, Kaliakatsos & Abbott 2010; Iacovacci et al. 2024) and microbial contamination, infection, biofilm formation and ecology (DiLuzio et al. 2005; Rusconi & Stocker 2015; Junot et al. 2019; Mathijssen et al. 2019). In turn, the prevalence and utility of background flows in microswimmer environments has motivated numerous theoretical studies investigating how background flows alter the swimmer dynamics. These range from studies closely aligned to observed microswimmer behaviours (Kantsler et al. 2014; Ishimoto & Gaffney 2015; Junot et al. 2019) to more theoretical investigations that analyse the general dynamics and mechanics exhibited by theoretical models (Hill et al. 2007; Zöttl & Stark 2012, 2014; Chengala, Hondzo & Sheng 2013; Ishimoto 2017, 2023).

However, even among the theoretical studies, there has been a focus on specific background flows, especially Poiseuille and shear flows (Zöttl & Stark 2012; Chengala et al. 2013; Ishimoto & Gaffney 2015; Junot et al. 2019; Ishimoto 2023). Such flows are often well-motivated, since Poiseuille flows are common in a confined microgeometries and shear flows are a somewhat general approximation close to surfaces, noting that many swimmers accumulate near surfaces (Woolley 2003; Lauga et al. 2006). This focus on candidate flows prompts the broader question of how do microswimmers respond to more general background flows, especially in the absence of a confining geometry or a nearby surface. This is all the more relevant given individual models for swimmer dynamics are often and increasingly integrated into the development of models for collective behaviour, for example the works of Saintillan & Shelley (2013), Ezhilan, Shelley & Saintillan (2013) and Junot et al. (2019).

Consequently, a pertinent generalisation of previous studies is to document and classify the behaviour of microswimmers in more general flows. We pursue this in terms of the features of the flow and the swimmer's shape deformation cycle, also termed a gait cycle. However, the potential scope is unwieldy in full generality due to the diversity of possible flows and possible microswimmers. Thus, in this study, we restrict ourselves to planar, linear flows where, at most, we consider only spatially constant flows perpendicular to the plane of motion. The restriction to linear flows entails that the flow decomposes into a translation, rigid body rotation, and a pure strain, with the well-studied shear flow constituting an edge case in this general exploration. Despite such restrictions, and further constraints detailed below, the consideration of swimmers in more general linear planar flows with a focus on analytical results provides the novelty of our investigation, as emphasised by the observation, for example, that mathematical precision is required to balance the flow angular velocity and rate of strain to generate a pure shear flow. Hence, previous detailed studies of swimmers in shear flow may in fact only represent edge cases for the possible dynamical behaviours.

Additionally, we restrict the range of possible swimmers to maintain tractability. One assumption is that the deformation cycle of the swimmer is sufficiently robust to be unchanged by the background flow. A further simplification that pertains to numerous

microswimmers is high inefficiency: to swim, non-reciprocal body deformations are required for actuation, with the period of deformation giving one time scale, whilst the time to swim a body length gives a second time scale, with the latter being much longer in the case of swimmer inefficiency. This separation of time scales can be readily seen in biological swimmers, for instance sperm (Smith *et al.* 2009), as well as many theoretical studies of idealised swimmers (Curtis & Gaffney 2013; Ishimoto & Gaffney 2014; Pak & Lauga 2015). Hence, we assume such swimmer inefficiency, especially as it presents a means to extensively simplify the resulting equations of motion using the method of multiple time scales, as has been applied to the theory of microswimmers in numerous diverse contexts (e.g. Ma, Pujara & Thiffeault 2022; Ventrella *et al.* 2023; Walker, Ishimoto & Gaffney 2023; Dalwadi *et al.* 2024a, *b*; Dalwadi 2025).

We also assume that the velocity scale of the background flow is not extensively greater than the velocity scale of net swimming, so that the swimmer is not simply washed out. Nonetheless, we do relax this assumption for investigations of reciprocal swimming, where the swimmer oscillates back and forth with no net motion in a quiescent fluid, to consider whether or not the interaction of background flows with oscillatory swimmer motion can induce overall motility. We also allow for the prospect of oscillations of the background flow, noting there is an emerging interest in how swimmers interact with oscillating background flows (Hope *et al.* 2016*a*; Jo *et al.* 2016; Moreau & Ishimoto 2021; Ma *et al.* 2022; Ventrella *et al.* 2023), especially in scenarios where an inefficient swimmer makes progress in a background flow oscillating with a frequency commensurate with that of the swimmer deformation (Morita *et al.* 2018*a,b*; Ishikawa, Morita & Omori 2022). The latter is particularly relevant to the current study and, thus, we incorporate background fluid flow oscillations with a frequency of the order of magnitude of the fast swimmer shape deformations.

A more technical constraint is the restriction to swimmers with sufficient symmetry to ensure that the impact of the fluid rate of strain on the swimmer simplifies. In generality, this would be governed by two rank-three tensors (Kim & Karrila 2005) and thus $2 \times 3^3 = 54$ degrees of freedom, each of which is a periodic function of the fast time scale since the swimmer is changing shape periodically to effect swimming. With symmetry constraints on the swimmer, including those required to ensure that simplifications from the planar symmetry of the flow are retained, these degrees of freedom can be reduced dramatically (Ishimoto 2020b), which we document in more detail in § 2.2. For instance, swimmers that are bodies of revolution throughout their deformation cycle are special cases of the results considered below. However, we also explore the consequences of weaker symmetry constraints. For example, the presence of a swimmer-fixed axis with swimmer shape invariance to rotations of $2\pi/3$ about this axis, together with three invariant reflection planes containing the body fixed axis, throughout the swimmer shape deformation cycle is sufficient to apply the results of the analysis below, and other relatively low-symmetry shape deformations are considered too.

Since spheres and spheroids fall into the symmetry classification we study, a sphere or a spheroid with a surface velocity slip profile, known as a spherical or spheroidal squirmer, is captured in our theory. Such a squirmer is not only a reasonable model of many ciliates and *Volvox*, but has also been used as a canonical theoretical model both for biological and artificial microswimmers (Ishikawa 2024). The symmetry class studied here also includes particles and swimmers with discrete rotational symmetry (Fries, Einarsson & Mehlig 2017), such as diatoms with regular *n*-gonal prism shape and radiolarians with regular polygonal pyramid shape (Gordon *et al.* 2009; Ishimoto 2020*b*). A simple uniform helix also falls in the symmetry class of this study, while a bacterial model composed of a helix coupled to a rigid spheroid is excluded due to insufficient reflection symmetry.

In summary, our objectives are to analyse and classify the planar dynamics of inertialess but inefficient microswimmers in linear background flows. In doing so, we retain sufficient generality to consider rotational, irrotational, and shear flows as special cases, with the general linear planar flow still amenable to analysis, even with flow oscillations on the same fast time scale as the swimmer's gait. From the perspective of rotational dynamics, we are particularly interested in whether a swimmer will tumble indefinitely, rock back and forth or asymptote to a fixed angle, including how this is contingent on the properties of the both the swimmer and the flow, as well as interactions between them. Similar questions arise in considering translational dynamics, especially whether the swimmer inexorably drifts indefinitely across flow pathlines or settles into periodic orbits, and also whether swimmer-flow interactions can generate net motility for reciprocal swimmers and, thus, circumvent Purcell's scallop theorem (Purcell 1977). In turn, this allows us to consider to what extent, and how, a microswimmer may control its trajectory within a general planar linear flow.

We pursue these objectives by first formulating the governing equations in § 2. Then, utilising the assumption of inefficiency via its concomitant separation of time scales between swimmer undulation and motion, the governing equations are simplified in § 3 and general features of the resulting solutions are examined, including a classification of the angular dynamics in § 4 and the translational dynamics in § 5. This is followed by numerical and theoretical investigations of special cases in § 6, with a focus on more symmetric swimmers and specific fluid flows for concreteness. Finally, we conclude with a general classification and summary in § 7, which readers may wish to review for the main findings before proceeding to the technical details below.

2. Governing equations

We derive the governing equations for inefficient swimmers undergoing rapid shape changing in planar background flows, with sufficient swimmer symmetry to render the swimmer motion planar and to ensure that interaction between the swimmer and the background flow rate of strain remains tractable. We additionally impose the following constraints: the swimmer mechanics and background flow are effectively inertialess; the swimmer shape is independent of the background flow; the swimmer shape oscillates on a fast time scale relative to the time scale of its net motion, with suitable generalisation if there is reciprocal swimming and, thus, no net motion; the background velocity field is a planar, incompressible Stokes flow that may in general oscillate on the fast time scale, commensurate with the time scale of the swimmer deformation oscillations. Whenever the background flow oscillates, for technical simplicity we additionally assume that the ratio of the flow oscillation period and the swimmer gait period is rational, with the overall period (the time for both the swimmer and the flow to return to the same phase) remaining a fast time scale.

With these assumptions, we immediately non-dimensionalise, with the viscosity scaled to unity by a choice of the pressure scale. In addition, we use the velocity, length and time scales of the background flow,

$$U_{bck}, \quad L_{bck}, \quad \tau_b = \frac{L_{bck}}{U_{bck}},$$
 (2.1)

respectively, to remove the remaining dimensions, thus generating the non-dimensional framework for the governing equations that we work with below. The non-dimensional background flow is denoted by u^* . As an example, consider a non-dimensionalised planar linear shear flow of the form

$$\boldsymbol{u}^*(\boldsymbol{x}, T) = \gamma(T)\gamma \boldsymbol{e}_1, \tag{2.2}$$

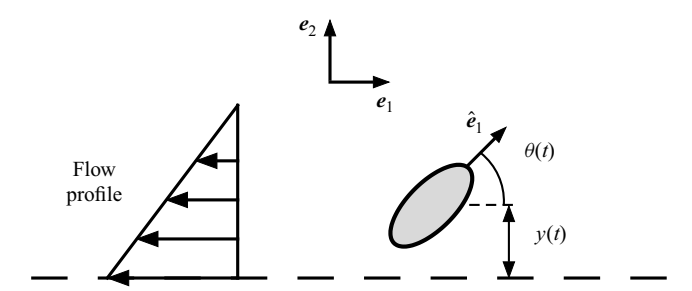


Figure 1. We illustrate a model swimmer in a planar, unidirectional, linear flow in the x-direction (e_1) and varying in the y-direction (e_2) , with the swimmer moving in the xy-plane. The swimmer orientation in the plane is captured via the unit vector \hat{e}_1 , which makes an angle θ with the e_1 axis.

at a fixed instant in time, as depicted in figure 1, with $\{e_1, e_2, e_3\}$ representing an inertial frame Cartesian basis for coordinates x, y, z with z out of the plane of the flow. Here, the non-dimensional shear rate, $\gamma(T)$, would be unity for shear that does not vary in time but, here, we allow it to oscillate on the fast time scale. This is represented by a dependence on a fast time variable T, associated with the swimmer gait oscillation and possible flow oscillation so that $T = 2\pi$ corresponds to one fast period. In turn, T is related to the slow time variable, t, via

$$T = \omega t, \quad \omega \gg 1.$$
 (2.3)

We also require t to be commensurate with the net swimming time scale, so that τ_b is of the order of the time it takes for the swimmer to have a net translation of a body length, so that the swimmer is not washed out by the flow. This also immediately satisfies our assumption that the swimmer is inefficient given $\omega \gg 1$, and can be viewed as the definition of inefficiency. However, a minor refinement is needed when considering the time scales for reciprocal swimmers, which never translate a body length in a quiescent fluid. In particular, reciprocal swimmers are, in a suitable sense, maximally inefficient but the net swimming time scale is nevertheless ill-defined. Thus, above, we have not used the time to swim one body length for non-dimensionalisation and, in addition, for reciprocal swimmers we relax the requirement that τ_b is on the time scale needed for the swimmer to translate a body length.

2.1. Flow kinematics and general governing equations

With the time scales defined, we can proceed to consider the background flow in detail and derive the governing equations for the rotational and translation dynamics of the swimmer. We have $\mathbf{x} = x\mathbf{e}_1 + y\mathbf{e}_2 + z\mathbf{e}_3$ as the non-dimensional position of a general point with respect to the laboratory-fixed basis, $\{\mathbf{e}_1, \mathbf{e}_2, \mathbf{e}_3\}$; analogously, the swimmer-fixed frame has a basis given by $\{\hat{\mathbf{e}}_1, \hat{\mathbf{e}}_2, \hat{\mathbf{e}}_3\}$ with its origin \mathbf{x}_c at the centroid of the swimmer. As further detailed below, the swimmer is taken to possess a body-fixed symmetry axis throughout its deformation cycle, which we take to be aligned in the body-fixed direction $\hat{\mathbf{e}}_1$. Noting the assumptions of flow planarity and sufficient swimmer symmetry to ensure planar motility (detailed below) we can, with suitable initial conditions implicitly assumed, take the swimmer axis of symmetry to lie in the plane of the flow which, without loss, is the xy-plane of the inertial frame. Note that this entails that $\hat{\mathbf{e}}_1$ also lies in this plane. Hence, we have the simple relations between the basis vectors

$$\hat{\boldsymbol{e}}_1 = \cos\theta \boldsymbol{e}_1 + \sin\theta \boldsymbol{e}_2, \quad \hat{\boldsymbol{e}}_2 = -\sin\theta \boldsymbol{e}_1 + \cos\theta \boldsymbol{e}_2, \quad \hat{\boldsymbol{e}}_3 = \boldsymbol{e}_3, \tag{2.4}$$

with θ as depicted in figure 1. In practice, this alignment also requires stability of planar swimming, which we do not explore in this work.

Neglecting the influence of the swimmer on the flow (so that no-slip conditions on the swimmer surface are not imposed), we denote the linear, planar, non-dimensional background flow field as $u^*(x, T)$ with rate of strain and angular velocity given by (Bachelor 1967)

$$\boldsymbol{E}^*(T) = \frac{1}{2} \left[\nabla \boldsymbol{u}^* + (\nabla \boldsymbol{u}^*)^\top \right], \quad \boldsymbol{\Omega}^*(T) = \frac{1}{2} \nabla \wedge \boldsymbol{u}^*, \tag{2.5}$$

respectively, where \cdot^{\top} denotes the transpose. As above, the prospect of rapid background flow oscillation is indicated by the fast time variable dependence of the rate of strain and angular velocity while, by the linearity of the flow, we have Ω^* and E^* are independent of spatial location. As the flow is planar we have the further simplifications

$$\boldsymbol{\Omega}^*(T) = \Omega^*(T)\hat{\boldsymbol{e}}_3 = \Omega^*(T)\boldsymbol{e}_3, \quad \Omega^*(T) = \frac{1}{2}\boldsymbol{e}_3 \cdot \nabla \wedge \boldsymbol{u}^*. \tag{2.6}$$

Further, we have that the rate of strain tensor, \boldsymbol{E}^* , can be written with respect to the laboratory basis as

$$\mathbf{E}^* = \begin{bmatrix} E_{11}^*(T) & E_{12}^*(T) & 0 \\ E_{12}^*(T) & -E_{11}^*(T) & 0 \\ 0 & 0 & 0 \end{bmatrix}, \tag{2.7}$$

noting that symmetry and flow incompressibility entail that only two degrees of freedom remain. In the same laboratory reference frame, the background flow takes the explicit form

$$u^{*}(x, T) = u_{tr}^{*}(T) + \underbrace{(-y\boldsymbol{e}_{1} + x\boldsymbol{e}_{2})\Omega^{*}(T)}_{\text{pure rotation}}$$

$$+ \underbrace{(x\boldsymbol{e}_{1} - y\boldsymbol{e}_{2})E_{11}^{*}(T) + (y\boldsymbol{e}_{1} + x\boldsymbol{e}_{2})E_{12}^{*}(T)}_{\text{pure strain}}$$

$$= u_{tr}^{*}(T) + \Omega^{*}(T) \wedge x + \boldsymbol{E}^{*}(T)x, \qquad (2.8)$$

where $u_{tr}^*(T)$ is a translational flow that has no spatial dependence. It is useful to note that velocity field satisfies the identity

$$\boldsymbol{u}^{*}(\boldsymbol{x},T) = \boldsymbol{u}_{c}^{*} + \boldsymbol{\Omega}^{*}(T) \wedge (\boldsymbol{x} - \boldsymbol{x}_{c}) + \boldsymbol{E}^{*}(T)(\boldsymbol{x} - \boldsymbol{x}_{c})$$
 (2.9)

by linearity, where $u_c^* = u^*(x_c, T)$ is the background flow at the centroid x_c of the swimmer.

With the background flow specified, we show in Appendix A that the planar motion of the swimmer is governed by

$$\frac{\mathrm{d}\boldsymbol{x}_c}{\mathrm{d}t} = \boldsymbol{u}_c^* + [V + \omega U(T)]\,\hat{\boldsymbol{e}}_1 - \tilde{\boldsymbol{g}}\boldsymbol{E}^*,\tag{2.10}$$

$$\dot{\theta}\boldsymbol{e}_{3} = \dot{\theta}\hat{\boldsymbol{e}}_{3} = \left[\Omega^{*}(T) + \Omega(T) + \omega\Omega_{f}(T)\right]\hat{\boldsymbol{e}}_{3} - \tilde{\boldsymbol{h}}\boldsymbol{E}^{*}.$$
(2.11)

Here, $\omega U(T)$, V and $\omega \Omega_f(T) + \Omega(T)$ are the oscillatory swimming speed, average progressive swimming speed and rate of rotation of the swimmer in the absence of any background flow, each of which are assumed to be given. Note that we have decomposed the latter into a fast, zero-mean $O(\omega)$ component $\Omega_f(T)$ and an O(1) component $\Omega(T)$ for later convenience. As described in detail in Appendix A, we assume $V \sim O(1)$ and

 $\omega U(T) \sim O(\omega)$, with the average of U(T) evaluating to zero over a period of the fast oscillation, $T=2\pi$. This is commensurate with the notion of swimmer inefficiency: swimmer variations that occur on the fast scale do not generate net motion on the fast scale. Later, during our asymptotic analysis of the translational equation of (2.10), we will see that this setting necessitates an additional constraint on U(T) and $\Omega_f(T)$, in that a particular nonlinear combination of these functions must have an average that is $O(1/\omega)$ (see the discussion that follows (3.22) for more details). Notably, relaxing these assumptions of inefficiency will lead to swimmers that, at leading order, do not meaningfully interact with the flow.

Note that setting u_c^* , \boldsymbol{E}^* and Ω^* to zero gives the equations of motion in the absence of flow. The terms $\tilde{\boldsymbol{g}}$ and $\tilde{\boldsymbol{h}}$ are rank three tensors that capture how the rate of strain of the background influences the swimmer dynamics. The assumption of planarity requires $\tilde{\boldsymbol{h}}\boldsymbol{E}^* \parallel \hat{\boldsymbol{e}}_3$, which we impose by constraining the swimmer shape throughout its gait cycle to have sufficient symmetry. However, we remark that this framework retains validity even when $\tilde{\boldsymbol{g}}\boldsymbol{E}^*$ has a component in the $\hat{\boldsymbol{e}}_3 = \boldsymbol{e}_3$ direction, so we do not disallow this prospect a priori. Here and throughout, all angular velocities are constrained to the $\hat{\boldsymbol{e}}_3 = \boldsymbol{e}_3$ direction by the assumption of planarity.

Below, we simplify these equations of motion by enforcing geometrical symmetries of the swimmer. The generality of the resulting derivations and equations naturally requires a relatively large number of parameters and variables. Hence, we summarise these in tables 1 and 2 for reference, together with the parameters and variables already introduced.

2.2. Simplified governing equations

In order to be consistent with our assumption of planarity, we must restrict ourselves to particular classes of swimmer geometry. In full generality, this is necessarily technical and requires significant notation. A reader seeking a concrete example might consider the swimmer to be a body of revolution with fore–aft symmetry, though we remark that much more general geometries are admissible within the present framework. Below, we elaborate on the details of some additional cases, though these can be safely skipped if one is willing to accept the presence of the time-dependent geometrical parameters B(T), $\lambda_5(T)$, $\eta_2(T)$, $\eta_3(T)$ and $\eta_4(T)$ in the explicit and simplified governing equations,

$$\frac{\mathrm{d}\boldsymbol{x}_{c}}{\mathrm{d}t} = \boldsymbol{u}_{c}^{*} + [V + \omega U(T)] \,\hat{\boldsymbol{e}}_{1} - \eta_{2}(T) [\hat{\boldsymbol{e}}_{1}^{\top} \boldsymbol{E}^{*}(T) \hat{\boldsymbol{e}}_{2}] \hat{\boldsymbol{e}}_{3}
+ \eta_{3}(T) \boldsymbol{B}_{0}(T, \sin 2\theta, \cos 2\theta) \hat{\boldsymbol{e}}_{1} - \eta_{4}(T) [\hat{\boldsymbol{e}}_{2}^{\top} \boldsymbol{E}^{*}(T) \hat{\boldsymbol{e}}_{2}] \hat{\boldsymbol{e}}_{2},$$

$$\frac{\mathrm{d}\theta}{\mathrm{d}t} = \Omega^{*}(T) + \omega \Omega_{f}(T) + \Omega(T) + [\lambda_{5}(T) E_{12}^{*}(T) - B(T) E_{11}^{*}(T)] \sin 2\theta
+ [\lambda_{5}(T) E_{11}^{*}(T) + B(T) E_{12}^{*}(T)] \cos 2\theta.$$
(2.13)

Here, B(T) is the Bretherton parameter and, using $c \equiv \cos 2\theta$ and $s \equiv \sin 2\theta$, we have that $B_0(T, \sin 2\theta, \cos 2\theta)$ is given by

$$\mathbf{B}_{0}(T, \sin 2\theta, \cos 2\theta) = \mathbf{E}^{*} - [E_{11}^{*}(T)\cos 2\theta + E_{12}^{*}(T)\sin 2\theta](\mathbf{e}_{1}\mathbf{e}_{1}^{\top} + \mathbf{e}_{2}\mathbf{e}_{2}^{\top})
= \begin{bmatrix} E_{11}^{*}(T)(1-c) - E_{12}^{*}(T)s & E_{12}^{*}(T) & 0 \\ E_{12}^{*}(T) & -[E_{11}^{*}(T)(1+c) + E_{12}^{*}(T)s] & 0 \\ 0 & 0 \end{bmatrix}, (2.14)$$

where the final expression is with respect to the laboratory basis. In the remainder of this section, we explicitly describe the construction of these governing equations from (2.10); we continue with an analysis of these equations in § 3.

Parameter/Variable	Description
$U_{bck}, L_{bck}, \tau_b = L_{bck}/U_{bck}$	Dimensional velocity, length and time scale of the background flow; see (2.1).
$t, T = \omega t$	Slow and fast time scales, respectively, with $\omega \gg 1$. See (2.3).
$\{e_1, e_2, e_3\}$	Laboratory-fixed basis. Section 2.1.
$\{\hat{\pmb{e}}_1, \hat{\pmb{e}}_2, \hat{\pmb{e}}_3\}$	Swimmer-fixed basis. Note $\hat{e}_3 = e_3$. See § 2.1.
θ	Swimmer orientation angle. See (2.4).
x, x_c	Field point and the swimmer centroid. See § 2.1.
$\boldsymbol{u}^*(T), \boldsymbol{E}^*(T), \boldsymbol{\Omega}^*(T) = \Omega^* \boldsymbol{e}_3$	Background flow, its rate of strain tensor and its angular velocity. See (2.17) and (2.5).
$\mathbf{\Omega}(T, 0) = \omega \Omega_f(T) \mathbf{e}_3 + \Omega(T) \mathbf{e}_3$	Angular velocity of the swimmer when $u^* = 0$, decomposed into fast and slow components. See (2.10) and (A4).
E_{ij}^*, \hat{E}_{ij}^*	Components of \boldsymbol{E}^* in the laboratory and swimmer frames. See (2.7), (2.15).
u_c^*, u_{tr}^*	Background flow at the swimmer centroid and its spatially constant contribution. See (2.9) and (2.8).
V, U(T)	Mean swimming speed and oscillatory swimming speed. See (2.10) and (A2).
$C_{nv}, C_{nh}, D_n, D_{nh}$	Types of helicoidal symmetry. See § 2.2.
$ ilde{oldsymbol{g}}, ilde{oldsymbol{h}}$	Rank 3 tensors capturing the impact of the rate of strain on motility. See (A11).
d_1, d_2, d_3, d_4, d_5	Vectors used to decompose $-\tilde{\boldsymbol{g}}\boldsymbol{E}^*$, $-\tilde{\boldsymbol{h}}\boldsymbol{E}^*$. See (2.17) and (2.2).
$\lambda_2, \lambda_5, \eta_2, \eta_3, \eta_4$	Coefficients of the decomposition of $-\tilde{g}E^*$ and $-\tilde{h}E^*$. See (2.17) and (2.2).
$B = -\lambda_2$	Bretherton shape parameter. See (2.17) and (2.2).
$\boldsymbol{B}_0(T,\theta)$	Matrix used to summarise translational equation of motion before multiple scales approximation. See (2.14).

Table 1. A list of parameters and variables used in the formulation of the governing equations, including the description of the background flow and the swimmer symmetries. All are non-dimensional except for the first row of scales used to non-dimensionalise the system. Note that the variable u_{tr}^* is overloaded and relative to either the 2-D flow plane or three-dimensional (3-D) more generally according to context, with the 3-D expression including the constant z-contribution to the background flow. Parameters and variables introduced in the appendices that do not appear in the main text are not listed.

2.3. Simplification of the governing equations and detailed geometrical constraints

In order to ensure that the swimmer only rotates in the plane of the flow, we immediately restrict consideration to swimmers whose shape throughout the gait cycle possesses a rotational symmetry of degree $n \ge 3$. That is, the swimmers possess a body fixed axis throughout the gait cycle such that there is a shape invariance to rotations around this axis of angle $2\pi/n$ (Ishimoto 2020b). In Shoenflies notation, such a body with n-fold rotational symmetry is denoted by C_n . In turn, the body symmetry enforces the constraints on the entries of the third-rank tensors, $\tilde{\mathbf{g}}$ and $\hat{\mathbf{h}}$, yielding another type of shape classification based on the symmetry of these tensors. This symmetry is a hydrodynamic symmetry and we refer the interested reader to the detailed definitions of Ishimoto (2020a, b, 2023) for further elaboration on this rich topic. With this C_n $(n \ge 3)$ body symmetry, Ishimoto (2020b) considers the structure of $-\tilde{\mathbf{g}}\mathbf{E}^*$ and $-\tilde{\mathbf{h}}\mathbf{E}^*$ and shows that a C_n $(n \ge 3)$ body has helicoidal symmetry of degree three, for which the body dynamics are explicitly written down in the same form. By taking $n \to \infty$, it is known that a simple helix

Parameter/Variable	Description
$x_0, \theta_0, x_1, \theta_1$	Leading-order and next-to-leading-order approximations to the swimmer centroid and orientation angle. See (3.17).
$a_{\dagger},b_{\dagger},b_{\ddagger},c_{\dagger},c_{\ddagger},a,b,c$	Terms summarising contributions to the angular equation of motion. Here a, b, c are fast time scale averages of $a_{\dagger}, b_{\ddagger}, c_{\ddagger}$. See (3.1), (3.2) and (3.10).
$p,q, heta_{00}$	Here $p = (b^2 + c^2 - a^2)^{1/2}$, $q = (a^2 - b^2 - c^2)^{1/2}$, $\theta_{00} = \theta(t = 0)$. See (3.16).
$ ilde{ heta}_0(t)$	Auxiliary function of the slow time scale used in leading-order angular solution. See (3.6).
$\Psi(T)$	Fast time scale integral of $\Omega_f(T)$. See (3.6).
$\tilde{\boldsymbol{e}}_{10}(\tilde{\theta}_0), \tilde{\boldsymbol{e}}_{20}(\tilde{\theta}_0)$	Vectors in the leading-order multiple scales approximation to $\hat{e}_1(\theta)$. See (3.19).
$U_c(T), U_s(T)$	Mean-subtracted products of gait and orientation. See (3.24).
n	Concise form of the coefficient of θ_1 in the translational governing equations, with $\mathbf{n} = -U_s(T)\tilde{\mathbf{e}}_{10} + U_c(T)\tilde{\mathbf{e}}_{20}$.
I_{Uc}, I_{Us}	Periodic, fast time scale integrals of U_c and U_s . See (3.28).
$\Lambda(T)$	Matrix used in summarising expansion of background flow. See (3.20).
\mathcal{L}, \mathcal{G}	Linear operator and image for the Fredholm alternative. See (3.31).
s_1, s_2, s_3, s_4	Spanning basis for the nullspace of the adjoint of \mathcal{L} . See (3.34).
χ	Here $\chi = a_{\dagger}(T) - b_{\ddagger}(T) \sin(2\tilde{\theta}_0) - c_{\ddagger} \cos(2\tilde{\theta}_0)$. See (3.12).
$F_1, F_2, G_1, G_2, H_1, H_2$	Linear functions of $\cos 2\tilde{\theta}_0$ and $\sin 2\tilde{\theta}_0$ summarising the form of the effective translational equations. See (3.38) to (3.40).
$C(\sin 2\tilde{\theta}_0, \cos 2\tilde{\theta}_0, \sin \tilde{\theta}_0, \cos \tilde{\theta}_0)$	Here $\tilde{\theta}_0$ -dependent vector within the translational equations and is linear in its arguments. See (3.46).
$\mathbf{A}, \mathbf{K} = \exp[\mathbf{A}t]$	Constant matrix and its exponential for the translational equation of motion and its solution. See (3.41) and (3.45).
$ u$, μ	Here $\nu = (\overline{E_{11}^*}^2 + \overline{E_{12}^*}^2 - \overline{\Omega^*}^2)^{1/2}$, $\mu = (\overline{\Omega^*}^2 - \overline{E_{11}^*}^2 - \overline{E_{12}^*}^2)^{1/2}$ describing the in-plane dynamics of the translational motion. See (3.44) <i>et seq</i> .
$\mathcal{A},\mathcal{B},\mathcal{K}$	Constants in the trajectory equation for an oscillatory shear background flow. See (6.16) and (6.18).

Table 2. A list of parameters and variables describing the multiscale simplifications and aspects of the explicit solutions to the governing equations for special cases. They are all non-dimensional. An overline of any variable refers to taking a temporal average over a period of the fast time scale, as defined by (3.7). Note that the variables \overline{x}_0 and Λ are overloaded and relative to either the 2-D flow plane, or 3-D more generally, according to context, with 3-D expressions, respectively, including the z-contribution to the leading-order swimmer centroid position and a trivial zero-padding in the third dimension when Λ acts on a 3-D vector. Parameters and variables introduced in the appendices that do not appear in the main text are not listed in this table.

approximately follows the same dynamical equations (Ishimoto 2020a). However, the helicoidal symmetry alone is not sufficient for our purposes. Thus, we closely follow Ishimoto (2020b) to determine $-\tilde{g}E^*$ and $-\tilde{h}E^*$, noting that additional simplifications will arise here from both the planar nature of the flow and the restriction of swimmer shapes to those for which $\tilde{h}E^* \parallel \hat{e}_3$. Before doing so, it is convenient to introduce the notation

$$\hat{\boldsymbol{E}}_{ij}^{*}(T,\sin 2\theta,\cos 2\theta) := \hat{\boldsymbol{e}}_{i}^{\mathsf{T}}\boldsymbol{E}^{*}(T)\hat{\boldsymbol{e}}_{j} = \hat{\boldsymbol{E}}_{ji}^{*}(T,\sin 2\theta,\cos 2\theta)$$
(2.15)

for $i, j \in \{1, 2, 3\}$. Explicitly, for $j \in \{1, 2, 3\}$ we have

$$\hat{E}_{11}^* = -\hat{E}_{22}^* = E_{11}^*(T)\cos 2\theta + E_{12}^*(T)\sin 2\theta, \tag{2.16a}$$

$$\hat{E}_{12}^* = E_{12}^*(T)\cos 2\theta - E_{11}^*(T)\sin 2\theta, \tag{2.16b}$$

$$\hat{E}_{3i}^* = 0, (2.16c)$$

each functions of T, $\sin 2\theta$ and $\cos 2\theta$. This corresponds to the rate of strain tensor expressed in the $\{\hat{e}_1, \hat{e}_2, \hat{e}_3\}$ basis. Later, we will make us of these definitions of \hat{E}_{ij}^* as functions of $\sin 2\theta$ and $\cos 2\theta$, wherein it will be appropriate to substitute θ for another angular variable.

With our assumptions and simplifications, we can now decompose $-\tilde{\mathbf{g}}\mathbf{E}^*$ and $-\tilde{\mathbf{h}}\mathbf{E}^*$ via

$$-\tilde{\mathbf{g}}\mathbf{E}^* = \eta_2(T)\mathbf{d}_2(T,\theta) + \eta_3(T)\mathbf{d}_3(T,\theta) + \eta_4(T)\mathbf{d}_4(T,\theta), \tag{2.17a}$$

$$-\tilde{\mathbf{h}}\mathbf{E}^* = \lambda_2(T)\mathbf{d}_2(T,\theta) + \lambda_5(T)\mathbf{d}_5(T,\theta)$$
 (2.17b)

with

$$d_2(T,\theta) = -\hat{E}_{12}^* \hat{e}_3, \quad d_3(T,\theta) = (\mathbf{E}^* - \hat{E}_{11}^* \mathbf{h}) \hat{e}_1, \tag{2.18a}$$

$$\mathbf{d}_4(T,\theta) = -\hat{E}_{22}^* \hat{\mathbf{e}}_2, \quad \mathbf{d}_5(T,\theta) = -\hat{E}_{22}^* \hat{\mathbf{e}}_3, \tag{2.18b}$$

where $\lambda_2(T) \equiv -B(T)$, $\lambda_5(T)$, $\eta_2(T)$, $\eta_3(T)$ and $\eta_4(T)$ are shape-dependent parameters. Notably, symmetries have to be imposed on the swimmer in order to ensure that there are no contributions to $-\tilde{\pmb{h}}\pmb{E}^*$ from $\pmb{d}_3(T,\theta)$ and $\pmb{d}_4(T,\theta)$, so that $\tilde{\pmb{h}}\pmb{E}^* \parallel \hat{\pmb{e}}_3$. For the swimmer shapes we consider throughout, this also ensures that $-\tilde{\pmb{g}}\pmb{E}^*$ has no contribution from $\pmb{d}_5(T,\theta)$ (Ishimoto 2020b). Thus, we do not consider the full range of shapes for which (2.17) is valid, but instead require additional restrictions. Particular examples of swimmer shapes with sufficient symmetry to be admissible within the present framework, together with the related restrictions on (2.17), are presented in detail in Appendix B for the interested reader. Finally, we note that for the simple canonical example of a body of revolution with fore–aft symmetry, there is extensive simplification, with $\lambda_5 = \eta_2 = \eta_3 = \eta_4 = 0$. Such a swimmer does not have the asymmetry needed to generate rotation in the absence of a flow, so that its angular velocity in the absence of flow, $\omega\Omega_f(T) + \Omega(T)$, is also zero.

3. Multiscale analysis in time-dependent flows

We proceed to use a multiscale analysis to simplify the governing equations, taking advantage of the separation of time scale arising from $\omega \gg 1$, so that ωt is fast time scale relative to t. As previously noted, we implicitly assume that the period of the fast time scale oscillations is a small integer number of periods of any background flow oscillation and swimmer deformation oscillation, including treadmilling, which ensures there is only one fast time scale.

3.1. Multiple scales for the angular dynamics

Defining

$$a_{\dagger}(T) = \Omega^*(T) + \Omega(T), \tag{3.1a}$$

$$b_{\dagger}(T) = B(T)E_{11}^{*}(T) - \lambda_{5}(T)E_{12}^{*}(T), \tag{3.1b}$$

$$c_{\dagger}(T) = -B(T)E_{12}^{*}(T) - \lambda_{5}(T)E_{11}^{*}(T), \tag{3.1c}$$

for notational convenience, the angular evolution equation becomes

$$\frac{\mathrm{d}\theta}{\mathrm{d}t} = \omega \Omega_f(T) + a_{\dagger}(T) - b_{\dagger}(T)\sin 2\theta - c_{\dagger}(T)\cos 2\theta, \tag{3.2}$$

which is decoupled from the equations for translational motion and thus may be treated in isolation.

To study this angular dynamics, we use the method of multiple time scales, exploiting $\omega \gg 1$. The slow time scale, t, is associated with the flow, and the fast time scale, $T = \omega t$, is associated with the swimmer deformation and treadmilling. Hence, the total time derivative decomposes via

$$\frac{\mathrm{d}}{\mathrm{d}t} = \frac{\partial}{\partial t} + \omega \frac{\partial}{\partial T}.\tag{3.3}$$

With a zero subscript denoting the leading order, we expand θ via

$$\theta = \theta_0(t, T) + \frac{1}{\omega}\theta_1(t, T) + \dots, \tag{3.4}$$

with $\theta_1(t, T)$ inheriting the 2π -periodicity of the fast time dynamics, as is standard in the multiple time scales method. Thus, at $O(\omega)$ and O(1) we have, respectively,

$$\theta_{0T} = \Omega_f(T), \tag{3.5a}$$

$$\theta_{1T} = -\theta_{0t} + a_{\dagger}(T) - b_{\dagger}(T)\sin 2\theta_0 - c_{\dagger}(T)\cos 2\theta_0. \tag{3.5b}$$

This gives

$$\theta_0(t,T) = \Psi(T) + \tilde{\theta}_0(t), \quad \Psi(T) = \int_0^T \Omega_f(S) \, \mathrm{d}S, \tag{3.6}$$

where $\tilde{\theta}_0(t)$ is an undetermined function of t alone. We denote fast time scale averages of functions that are 2π -periodic in the fast variable T using a bar, that is

$$\overline{Q} := \frac{1}{2\pi} \int_{T_0}^{T_0 + 2\pi} Q(t, T) dT = \frac{1}{2\pi} \int_0^{2\pi} Q(t, T) dT,$$
 (3.7)

where the T_0 dependence drops due to the periodicity in the fast variable. Noting that $\Psi(T)$ is 2π -periodic, as $\Omega_f(T)$ is 2π -periodic with zero mean, averaging (3.6) gives

$$\overline{\theta}_0(t) = \overline{\Psi} + \tilde{\theta}_0(t), \tag{3.8}$$

with $\overline{\Psi}$ a constant, so that $d\tilde{\theta}_0/dt = d\overline{\theta}_0/dt$.

Given (3.6), we expand

$$b_{\dagger}(T)\sin 2\theta_0 + c_{\dagger}(T)\cos 2\theta_0 = b_{\dagger}(T)\sin(2\tilde{\theta}_0 + 2\Psi) + c_{\dagger}(T)\cos(2\tilde{\theta}_0 + 2\Psi)$$
$$= b_{\dagger}(T)\sin(2\tilde{\theta}_0) + c_{\dagger}(T)\cos(2\tilde{\theta}_0), \tag{3.9}$$

where we define

$$b_{\ddagger}(T) = B(T)\hat{E}_{11}^{*}(T,\sin(2\Psi),\cos(2\Psi)) - \lambda_{5}(T)\hat{E}_{12}^{*}(T,\sin(2\Psi),\cos(2\Psi))$$
 (3.10a)

$$c_{\ddagger}(T) = -B(T)\hat{E}_{12}^{*}(T,\sin(2\Psi),\cos(2\Psi)) - \lambda_{5}(T)\hat{E}_{11}^{*}(T,\sin(2\Psi),\cos(2\Psi)) \quad (3.10b)$$

using the definitions of (2.16). Hence, the impact of the fast angular dynamics is that the contributions of the rate of strain tensor are taken only after a rotating the basis by an angle $\Psi(T)$.

As the only periodic homogeneous solution of (3.5b) for θ_1 is the constant solution, (3.9) and the Fredholm alternative theorem give

$$\int_0^{2\pi} \left\{ -\theta_{0t} + \chi(T) \right\} dT = 0, \tag{3.11}$$

defining

$$\chi(T) := a_{\dagger}(T) - b_{\pm}(T)\sin 2\tilde{\theta}_0 - c_{\pm}(T)\cos 2\tilde{\theta}_0 \tag{3.12}$$

for later convenience. Thus, the leading-order dynamics is governed by the simpler differential equation

$$\frac{\mathrm{d}\tilde{\theta}_0}{\mathrm{d}t} = a - b\sin 2\tilde{\theta}_0 - c\cos 2\tilde{\theta}_0, \quad a = \overline{a}_{\dagger}, \ b = \overline{b}_{\ddagger}, \ c = \overline{c}_{\ddagger}. \tag{3.13}$$

Note that we have defined a, b, c as the averages of a_{\dagger} , b_{\ddagger} , c_{\ddagger} , respectively, for ease of notation in what follows. These quantities will be key in exploring the emergent behaviour in § 4 to § 6. With the initial condition that

$$\tilde{\theta}_0(t=0) = \theta_0(t=0) = \theta_{00} \tag{3.14}$$

and the definitions

$$p = (b^2 + c^2 - a^2)^{1/2}, \quad q = (a^2 - b^2 - c^2)^{1/2},$$
 (3.15)

one can readily determine

$$\tan \tilde{\theta}_{0} = \begin{cases} \frac{p \tan \theta_{00} + [a - c - b \tan \theta_{00}] \tanh(pt)}{p + [b - (a + c) \tan \theta_{00}] \tanh(pt)}, & a^{2} < b^{2} + c^{2}, \\ \frac{\tan \theta_{00} + [a - c - b \tan \theta_{00}]t}{1 + [b - (a + c) \tan \theta_{00}]t}, & a = (b^{2} + c^{2})^{1/2}, \\ \frac{q \tan \theta_{00} + [a - c - b \tan \theta_{00}] \tan(qt)}{q + [b - (a + c) \tan \theta_{00}] \tan(qt)}, & a^{2} > b^{2} + c^{2}, \end{cases}$$
(3.16)

where the appropriate branches of arctan are chosen so that $\tilde{\theta}_0$ is continuous. Note that, by (3.8), this also gives the angular evolution of $\bar{\theta}_0(t)$ up to a constant shift.

3.2. Multiple scales for the translational dynamics

We proceed to consider the translational dynamics by applying the method of multiple scales to (2.12) using the expansions

$$\boldsymbol{x}_c = \boldsymbol{x}_0 + \frac{1}{\omega} \boldsymbol{x}_1 + \dots, \tag{3.17a}$$

$$\theta = \theta_0(t, T) + \frac{1}{\omega}\theta_1(t, T) + \dots = \tilde{\theta}_0(t) + \Psi(T) + \frac{1}{\omega}\theta_1(t, T) + \dots$$
 (3.17b)

Before doing so, it will prove convenient to expand the swimmer basis vectors of (2.4) in powers of ω using (3.17b). We write

$$\hat{\boldsymbol{e}}_{1}(\theta) = \cos \Psi \tilde{\boldsymbol{e}}_{10} + \sin \Psi \tilde{\boldsymbol{e}}_{20} + \frac{1}{\omega} \theta_{1} \left[-\sin \Psi \tilde{\boldsymbol{e}}_{10} + \cos \Psi \tilde{\boldsymbol{e}}_{20} \right] + O\left(\frac{1}{\omega^{2}}\right), \quad (3.18a)$$

$$\hat{\boldsymbol{e}}_{2}(\theta) = -\sin\Psi\tilde{\boldsymbol{e}}_{10} + \cos\Psi\tilde{\boldsymbol{e}}_{20} + O\left(\frac{1}{\omega}\right),\tag{3.18b}$$

defining

$$\tilde{\mathbf{e}}_{10}(t) = \cos \tilde{\theta}_0 \mathbf{e}_1 + \sin \tilde{\theta}_0 \mathbf{e}_2, \quad \tilde{\mathbf{e}}_{20}(t) = -\sin \tilde{\theta}_0 \mathbf{e}_1 + \cos \tilde{\theta}_0 \mathbf{e}_2. \tag{3.19}$$

We also write the translational equation in a more concise form by defining the matrix operator

$$\boldsymbol{\Lambda}(T) := \begin{bmatrix} E_{11}^*(T) & E_{12}^*(T) - \Omega^*(T) & 0 \\ E_{12}^*(T) + \Omega^*(T) & -E_{11}^*(T) & 0 \\ 0 & 0 & 0 \end{bmatrix}. \tag{3.20}$$

This allows us to write the background flow explicitly as an affine map of position, with

$$\boldsymbol{u}_{c}^{*} = \boldsymbol{u}_{tr}^{*}(T) + \boldsymbol{\Lambda}(T)\boldsymbol{x}_{c}, \tag{3.21}$$

so that the governing equation for the translational motion can be written as

$$\frac{\mathrm{d}\boldsymbol{x}_c}{\mathrm{d}t} = \boldsymbol{u}_{tr}^*(T) + \boldsymbol{\Lambda}(T)\boldsymbol{x}_c + [V + \omega U(T)]\,\hat{e}_1(\theta) - \tilde{\boldsymbol{g}}(\theta, T)\boldsymbol{E}^*(T). \tag{3.22}$$

Later, we will make use of the explicit expression derived for $-\tilde{g}E^*$ in (2.17), but we leave it implicit for now.

We are now in a position to discuss a further constraint imposed by our assumption of swimmer inefficiency. Whilst we have already assumed that $\overline{U} = \overline{\Omega_f} = 0$, for consistency we must also impose that the product of $\omega U(T)$ and $\hat{e}_1(\theta)$ in (3.22) does not generate terms that scale with ω ; otherwise, this would represent a fast effective swimming speed. In particular, noting the expansion of $\hat{e}_1(\theta)$ in (3.18), we additionally impose that

$$\overline{U}\cos\Psi, \ \overline{U}\sin\Psi = O\left(\frac{1}{\omega}\right),$$
 (3.23)

so that there is no average swimming at leading order in (3.22). This motivates us to define the 2π -periodic functions of the fast time scale

$$U_c(T) := U(T)\cos\Psi(T) - \overline{U}\cos\Psi, \qquad (3.24a)$$

$$U_s(T) := U(T)\sin\Psi(T) - \overline{U\sin\Psi}, \qquad (3.24b)$$

noting that $\overline{U_c} = \overline{U_s} = 0$. For later convenience, we write $V_{Uc} := \omega \overline{U} \cos \Psi$ and $V_{Us} := \omega \overline{U} \sin \overline{\Psi}$, both O(1) by assumption. These represent the average swimming speeds that arise due to the combination of angular oscillations and variations in linear swimming speed. With our notion of swimmer inefficiency now made precise, we write the translational governing equation of (3.22) as

$$\frac{\mathrm{d}\boldsymbol{x}_{c}}{\mathrm{d}t} = \boldsymbol{u}_{tr}^{*}(T) + \boldsymbol{\Lambda}(T)\boldsymbol{x}_{c} + \left[V\cos\boldsymbol{\Psi}(T) + V_{Uc}\right]\tilde{\boldsymbol{e}}_{10} + \left[V\sin\boldsymbol{\Psi}(T) + V_{Us}\right]\tilde{\boldsymbol{e}}_{20} + \boldsymbol{n}\theta_{1} + \omega\left[U_{c}(T)\tilde{\boldsymbol{e}}_{10} + U_{s}(T)\tilde{\boldsymbol{e}}_{20}\right] - \tilde{\boldsymbol{g}}(\theta, T)\boldsymbol{E}^{*}(T) + O\left(\frac{1}{\omega}\right), \quad (3.25)$$

writing $\mathbf{n} = -U_s(T)\tilde{\mathbf{e}}_{10} + U_c(T)\tilde{\mathbf{e}}_{20}$. Here, we have made use of (3.18) to make the dependence on the asymptotic approximation to θ explicit in all but $\tilde{\mathbf{g}}$.

With this expanded governing equation, we now apply the method of multiple scales as in the case of the angular dynamics. Transforming the time derivatives as in (3.3) and inserting the expansion of (3.17), we have the leading-order balance

$$\frac{\partial \mathbf{x}_0}{\partial T} = U_c(T)\tilde{\mathbf{e}}_{10} + U_s(T)\tilde{\mathbf{e}}_{20} \tag{3.26}$$

at $O(\omega)$. This has solution

$$\mathbf{x}_0 = I_{Uc}(T)\tilde{\mathbf{e}}_{10}(t) + I_{Us}(T)\tilde{\mathbf{e}}_{20}(t) + \overline{\mathbf{x}}_{0}(t), \tag{3.27}$$

defining the 2π -periodic functions

$$I_{Uc} := \int_0^T U_c(s) \, \mathrm{d}s - C_c,$$
 (3.28a)

$$I_{Us} := \int_0^T U_s(s) \, \mathrm{d}s - C_s, \tag{3.28b}$$

where the constants C_c and C_s are chosen such that $\overline{I_{Uc}} = \overline{I_{Us}} = 0$. Note that the periodicity of I_{Uc} and I_{Us} follows from $\overline{U_c} = \overline{U_s} = 0$, in turn a consequence of swimmer inefficiency and the definitions of (3.24). These functions capture the oscillatory translational motion that arises from interactions between angular oscillations and the rapidly varying speed U(T).

At next order, we have the more complex balance

$$\frac{\partial \mathbf{x}_{1}}{\partial T} + \frac{\partial \mathbf{x}_{0}}{\partial t} = \mathbf{u}_{tr}^{*}(T) + \mathbf{\Lambda}(T)\mathbf{x}_{0} + [V\cos\Psi(T) + V_{Uc}]\,\tilde{\mathbf{e}}_{10} + [V\sin\Psi(T) + V_{Us}]\,\tilde{\mathbf{e}}_{20} + \mathbf{n}\theta_{1} - \tilde{\mathbf{q}}(\tilde{\theta}_{0} + \Psi(T), T)\mathbf{E}^{*}(T). \tag{3.29}$$

To make progress via the Fredholm alternative, we consider the linear operator

$$\mathcal{L} := \begin{bmatrix} \frac{\partial}{\partial T} & 0 & 0 & -\boldsymbol{n} \cdot \boldsymbol{e}_1 \\ 0 & \frac{\partial}{\partial T} & 0 & -\boldsymbol{n} \cdot \boldsymbol{e}_2 \\ 0 & 0 & \frac{\partial}{\partial T} & 0 \\ 0 & 0 & 0 & \frac{\partial}{\partial T} \end{bmatrix}$$
(3.30)

and the system

$$\mathcal{L}\begin{bmatrix} \mathbf{x}_1 \\ \theta_1 \end{bmatrix} = \mathbf{\mathcal{G}},\tag{3.31}$$

with the forcing \mathcal{G} given by concatenating the remaining terms of (3.29) and the integrand of (3.11), the latter being the forcing of the analogous angular evolution equation. We seek periodic solutions of the homogeneous adjoint problem, $\mathcal{L}^*s = 0$, where

$$\mathcal{L}^* = -\begin{bmatrix} \frac{\partial}{\partial T} & 0 & 0 & 0\\ 0 & \frac{\partial}{\partial T} & 0 & 0\\ 0 & 0 & \frac{\partial}{\partial T} & 0\\ \boldsymbol{n} \cdot \boldsymbol{e}_1 & \boldsymbol{n} \cdot \boldsymbol{e}_2 & 0 & \frac{\partial}{\partial T} \end{bmatrix}$$
(3.32)

and we compute $-\mathbf{n} \cdot \mathbf{e}_1 = U_s(T) \cos \tilde{\theta}_0 + U_c(T) \sin \tilde{\theta}_0$ and $-\mathbf{n} \cdot \mathbf{e}_2 = U_s(T) \sin \tilde{\theta}_0 - U_c(T) \cos \tilde{\theta}_0$. Note that, in order for solutions of the original forced system to exist, we require that \mathcal{G} is orthogonal to the nullspace of \mathcal{L}^* , writing $\langle \cdot, \cdot \rangle$ for the appropriate inner product.

Solving the adjoint problem leads to

$$s = \begin{bmatrix} c_1 \\ c_2 \\ c_3 \\ c_1 \left[I_{Us}(T) \cos \tilde{\theta}_0 + I_{Uc}(T) \sin \tilde{\theta}_0 \right] + c_2 \left[I_{Us}(T) \sin \tilde{\theta}_0 - I_{Uc}(T) \cos \tilde{\theta}_0 \right] + c_4 \end{bmatrix},$$
(3.33)

written in terms of arbitrary constants c_1 , c_2 , c_3 and c_4 . Abusing notation to write e_4 for the angular direction here, we have the independent solutions

$$s_1 = e_1 + \left[I_{Us}(T) \cos \tilde{\theta}_0 + I_{Uc}(T) \sin \tilde{\theta}_0 \right] e_4, \tag{3.34a}$$

$$s_2 = e_2 + \left[I_{Us}(T) \sin \tilde{\theta}_0 - I_{Uc}(T) \cos \tilde{\theta}_0 \right] e_4, \tag{3.34b}$$

$$\mathbf{s}_3 = \mathbf{e}_3,\tag{3.34c}$$

$$\mathbf{s}_4 = \mathbf{e}_4. \tag{3.34d}$$

These s_i each generate a solvability condition for the system, which will yield governing equations for the components of the motion. Notice that $\langle s_4, \mathcal{G} \rangle = 0$ collapses onto the condition found in our analysis of the angular evolution in (3.11), so that these approaches are consistent.

All the out-of-plane motion is generated by $\langle s_3, \mathcal{G} \rangle = 0$, which leads to the evolution equation

$$\frac{d\overline{z}_0}{dt} = \overline{\boldsymbol{u}_{tr}^*} \cdot \boldsymbol{e}_3 - \overline{\tilde{\boldsymbol{g}}(\tilde{\theta}_0 + \Psi(T), T)} \boldsymbol{E}^*(T) \cdot \boldsymbol{e}_3. \tag{3.35}$$

This corresponds to constant translation out of the plane and, as we will see that there is no dependence on \bar{z}_0 in the other governing equations, these dynamics decouple. Thus, without loss of generality, we overload our notation and neglect e_3 components of all quantities in what follows.

With this simplification and overloaded notation, the solvability conditions $\langle s_1, \mathcal{G} \rangle = \langle s_2, \mathcal{G} \rangle = 0$ generate the equations of in-plane motion, which we write as

$$\frac{\mathrm{d}\overline{x}_{0}}{\mathrm{d}t} = \overline{\boldsymbol{u}_{tr}^{*}} + \overline{\boldsymbol{\Lambda}}\overline{x}_{0} + \overline{I_{Uc}}\boldsymbol{\Lambda}\tilde{\boldsymbol{e}}_{10} + \overline{I_{Us}}\boldsymbol{\Lambda}\tilde{\boldsymbol{e}}_{20} + \left[V\overline{\cos\Psi} + V_{Uc} + \overline{\chi}I_{Us}\right]\tilde{\boldsymbol{e}}_{10} + \left[V\overline{\sin\Psi} + V_{Us} - \overline{\chi}I_{Uc}\right]\tilde{\boldsymbol{e}}_{20} - \overline{\tilde{\boldsymbol{g}}}(\tilde{\theta}_{0} + \Psi, T)\boldsymbol{E}^{*}, \tag{3.36}$$

recalling the definition of $\chi(T)$ from (3.12). It remains to compute the average of the shape-flow interaction terms captured by

$$\overline{\tilde{\mathbf{g}}(\tilde{\theta}_0 + \Psi, T)\mathbf{E}^*}. \tag{3.37}$$

This can be done in a straightforward manner using the expressions and definitions of (2.12) and (3.18), though the calculation is somewhat lengthy and broadly uninformative. For the purpose of our analysis, it suffices to summarise these expressions simply in terms of a sum of \tilde{e}_{10} and \tilde{e}_{20} , weighted by functions that are in linear in $\cos 2\tilde{\theta}_0$, $\sin 2\tilde{\theta}_0$, with coefficients formed of nonlinear averages of shape parameters (η_3 and η_4), background flow strain rates E_{ij}^* , and the fast oscillations of the swimmer orientation through Ψ . We write the average contribution as

$$-\overline{\tilde{\boldsymbol{g}}(\tilde{\theta}_0 + \boldsymbol{\Psi}, T)\boldsymbol{E}^*} = F_1(\cos 2\tilde{\theta}_0, \sin 2\tilde{\theta}_0)\tilde{\boldsymbol{e}}_{10} + F_2(\cos 2\tilde{\theta}_0, \sin 2\tilde{\theta}_0)\tilde{\boldsymbol{e}}_{20}$$
(3.38)

for implicitly defined linear functions F_1 and F_2 . These, along with other terms in the effective governing equations, simplify extensively under the assumption of no fast angular oscillations ($\Omega_f \equiv 0$), as explored in detail in Appendix C.

With this, the governing equation looks to be sufficiently complex as to be unwieldy. However, it turns out that there are further simplifications to be made through seemingly serendipitous cancellation. For instance, gross cancellation occurs in the following summation:

$$\overline{I_{Uc}\Lambda}\tilde{\boldsymbol{e}}_{10} + \overline{I_{Us}\Lambda}\tilde{\boldsymbol{e}}_{20} + \overline{\chi I_{Us}}\tilde{\boldsymbol{e}}_{10} - \overline{\chi I_{Uc}}\tilde{\boldsymbol{e}}_{20} = \left[\Omega I_{Us} + G_1\right]\tilde{\boldsymbol{e}}_{10} + \left[-\overline{\Omega I_{Uc}} + G_2\right]\tilde{\boldsymbol{e}}_{20}, \tag{3.39}$$

with all terms involving Ω^* vanishing. The unspecified functions G_1 and G_2 are linear in $\cos 2\tilde{\theta}_0$ and $\sin 2\tilde{\theta}_0$, analogous to F_1 and F_2 . Writing $\mathbf{A} = \overline{\mathbf{\Lambda}}$ for notational convenience in what follows, this entails that the governing equation can be written in the significantly simplified form

$$\frac{\mathrm{d}\overline{x}_{0}}{\mathrm{d}t} = \overline{u_{tr}^{*}} + \mathbf{A}\overline{x}_{0} + \left[V\overline{\cos\Psi} + V_{Uc} + \overline{\Omega I_{Us}} + H_{1}(2\tilde{\theta}_{0})\right]\tilde{e}_{10}(\tilde{\theta}_{0})
+ \left[V\overline{\sin\Psi} + V_{Us} - \overline{\Omega I_{Uc}} + H_{2}(2\tilde{\theta}_{0})\right]\tilde{e}_{20}(\tilde{\theta}_{0}),$$
(3.40)

with $H_1 = F_1 + G_1$ and $H_2 = F_2 + G_2$. To emphasise the structure of these equations of motion, we have explicitly included any dependence on the angular dynamics. In particular, all other quantities (save for \overline{x}_0) are constants – effective quantities that have arisen from the systematic multiscale analysis. Thus, the motion consists of constant translation by the background flow, linear interaction with the background flow via $\mathbf{A} = \overline{\mathbf{A}}$, and an effective self-propelled swimming that is modulated by the average angular dynamics in a nonlinear fashion. In what follows, we set $\overline{u_{tr}^*} = \mathbf{0}$ by choice of reference frame without loss of generality and, thus, the solutions for the equations of motion below are relative to the mean translational component of the background flow.

Remarkably, further progress can be made now that the evolution of \overline{x}_0 is written in this form. To proceed, we recall that

$$\mathbf{A} = \overline{\mathbf{\Lambda}} = \begin{bmatrix} \overline{E_{11}^*} & \overline{E_{12}^*} - \overline{\Omega}^* \\ \overline{E_{12}^*} + \overline{\Omega}^* & -\overline{E_{11}^*} \end{bmatrix}. \tag{3.41}$$

We note that its eigenvalues are given by

$$\pm \left(\overline{E_{11}^*}^2 + \overline{E_{12}^*}^2 - \overline{\Omega^*}^2\right)^{1/2} \tag{3.42}$$

and that

$$\mathbf{A}^2 = \left(\overline{E_{11}^*}^2 + \overline{E_{12}^*}^2 - \overline{\Omega^*}^2\right)\mathbf{I},\tag{3.43}$$

as is most readily deduced from the Cayley-Hamilton theorem. Hence, with the definitions

$$\nu := \left(\overline{E_{11}^*}^2 + \overline{E_{12}^*}^2 - \overline{\Omega^*}^2\right)^{1/2}, \quad \mu := \left(\overline{\Omega^*}^2 - \overline{E_{11}^*}^2 - \overline{E_{12}^*}^2\right)^{1/2}, \quad (3.44)$$

we can compute $\exp[\mathbf{A}t]$ to give

$$\mathbf{K}(t) := \exp[\mathbf{A}t] = \begin{cases} \cosh(\nu t)\mathbf{I} + \frac{1}{\nu}\sinh(\nu t)\mathbf{A}, & \overline{E_{11}^*}^2 + \overline{E_{12}^*}^2 > \overline{\Omega}^*^2, \\ \mathbf{I} + \mathbf{A}t, & \overline{E_{11}^*}^2 + \overline{E_{12}^*}^2 = \overline{\Omega}^*^2, \\ \cos(\mu t)\mathbf{I} + \frac{1}{\mu}\sin(\mu t)\mathbf{A}, & \overline{E_{11}^*}^2 + \overline{E_{12}^*}^2 < \overline{\Omega}^*^2. \end{cases}$$
(3.45)

The effective rates ν and μ capture the extent to which the rate of strain and the angular velocity of the background flow dominate one another, respectively. Note that at most one of ν and μ is real and non-zero for a given background flow.

Thus, solving (3.40) in terms of K and its convolution reveals

$$\overline{\boldsymbol{x}}_{0}(t) = \boldsymbol{K}(t)\overline{\boldsymbol{x}}_{0}(t=0) + \int_{0}^{t} \boldsymbol{K}(t-s)\boldsymbol{C}(\sin 2\tilde{\theta}_{0}(s), \cos 2\tilde{\theta}_{0}(s), \sin \tilde{\theta}_{0}(s), \cos \tilde{\theta}_{0}(s)) \, \mathrm{d}s, \qquad (3.46)$$

where we define

$$C := \left[V \overline{\cos \Psi} + V_{Uc} + \overline{\Omega I_{Us}} + H_1(2\tilde{\theta}_0) \right] \tilde{e}_{10}(\tilde{\theta}_0)$$

$$+ \left[V \overline{\sin \Psi} + V_{Us} - \overline{\Omega I_{Uc}} + H_2(2\tilde{\theta}_0) \right] \tilde{e}_{20}(\tilde{\theta}_0),$$
(3.47)

with H_1 and H_2 linear in $\cos 2\tilde{\theta}_0$ and $\sin 2\tilde{\theta}_0$.

4. Classification of rotational dynamics

Numerous deductions can be made from both the leading-order multiple scales solution for θ in (3.16) and for $x_0(t, T)$ and $\overline{x}_0(t)$ in (3.46). Such conclusions concern whether the swimmer rotational dynamics asymptotes to rocking, tumbling or a steady angle, and whether there is inexorable drift or oscillation in the translational dynamics.

The rotational dynamics for a rapidly deforming planar swimmer within a planar linear flow, with a possible fast oscillation, is given by (3.16). If we assume that $a^2 > b^2 + c^2$, we have

$$\tilde{\theta}_0 = \arctan\left(\frac{q \tan \theta_{00} + [a - c - b \tan \theta_{00}] \tan(qt)}{q + [b - (a + c) \tan \theta_{00}] \tan(qt)}\right),\tag{4.1}$$

where $q = (a^2 - b^2 - c^2)^{1/2}$ and θ_{00} is the initial value at t = 0. Note that there is a potential degenerate edge case with

$$a - c - b \tan \theta_{00} = 0 = b - (a + c) \tan \theta_{00},$$
 (4.2)

which would give $\tilde{\theta}_0 = \theta_{00}$ for all time. However, eliminating $\tan \theta_{00}$ in favour of a, b, c immediately yields $a^2 = b^2 + c^2$, violating our assumption. Thus, this degeneracy cannot be realised. Similarly, other degenerate cases lie out of reach, such as setting the numerator equal to zero in (4.1), which requires $\tan \theta_{00} = 0$ and a = c, once more violating $a^2 > b^2 + c^2$.

This rotational dynamics corresponds to a continuous tumble (rather than rocking back and forth). To see this, note that within the expression for $\tilde{\theta}_0$ given by (4.1), we have $\tan(qt)$ increasing in time monotonically, and the right-hand side is monotonic in $\tan(qt)$ (noting that we have excluded degenerate cases where the expression is constant). Thus, the jump in arctan to maintain continuity as qt passes though $\pi/2 + n\pi$ for some integer

n is always in the same direction, so that $\tilde{\theta}_0$ changes monotonically with increasing time. The non-dimensional period of the tumbling is given by

$$\frac{2\pi}{q},\tag{4.3}$$

with $q=(a^2-b^2-c^2)^{1/2}$ once more. The factor of two in the numerator arises because each jump to a new branch of arctan results in an increase in $\tilde{\theta}_0$ by π once qt propagates across the new branch, so that propagation across two branches is required to increase $\tilde{\theta}_0$ by a full rotation of 2π .

With this, and noting that the long-time limits of the other cases of (3.16) asymptote to a fixed angle, we thus have a necessary and sufficient condition for the swimmers of § 2 (with the symmetries of § 2.2) to tumble. In particular, endless tumbling is guaranteed precisely when $a^2 > b^2 + c^2$, that is

$$\begin{split} \left[\overline{\Omega^*(T) + \Omega(T)} \right]^2 \\ > & \left[\overline{B(T) \hat{E}_{11}^*(T, \sin 2\Psi, \cos 2\Psi) - \lambda_5(T) \hat{E}_{12}^*(T, \sin 2\Psi, \cos 2\Psi)} \right]^2 \\ + & \left[\overline{B(T) \hat{E}_{12}^*(T, \sin 2\Psi, \cos 2\Psi) + \lambda_5(T) \hat{E}_{11}^*(T, \sin 2\Psi, \cos 2\Psi)} \right]^2. \end{split} \tag{4.4}$$

For all bodies of § 2.2, except those that possess only the C_3 symmetry within the gait cycle, this reduces to

$$\left[\frac{\Omega^*(T) + \Omega(T)}{B(T)\hat{E}_{11}^*(T,\sin 2\Psi,\cos 2\Psi)}\right]^2 + \left[\frac{B(T)\hat{E}_{12}^*(T,\sin 2\Psi,\cos 2\Psi)}{B(T)\hat{E}_{12}^*(T,\sin 2\Psi,\cos 2\Psi)}\right]^2.$$
(4.5)

For any body of § 2.2 that also possesses fore—aft symmetry throughout the gait cycle, the condition further reduces to

$$\left[\overline{\Omega^*(T)}\right]^2 > \left[\overline{B(T)E_{11}^*(T)}\right]^2 + \left[\overline{B(T)E_{12}^*(T)}\right]^2. \tag{4.6}$$

This latter relation readily collapses onto $B^2 < 1$ if the particle is rigid and the flow is taken to be a simple, time-independent shear, in line with the classical results of Jeffery (1922) and Bretherton (1962). Notably, none of these criteria depend in any way on the translational swimming motility, with no dependence on V nor U(T).

Each of these conditions signifies that tumbling occurs once the angular forcing

$$\left[\overline{\Omega^*(T) + \Omega(T)}\right]^2 \tag{4.7}$$

is sufficiently high, where the threshold for tumbling depends on the details of the interactions between the deformation of the swimmer and the rate of shear experienced by the swimmer, accounting for any fast time scale changes in its orientation via the angle $\Psi(T)$. Notably, rocking never occurs in the swimmer system: in every case of (3.16), the swimmer angle never oscillates back and forth without whole turns. Instead, we have that the swimmer either tumbles or its orientation asymptotes to a fixed angle. This is in distinct contrast to the behaviour of a simple pendulum, where whole turns are replaced by rocking as the forcing is reduced.

Furthermore, if the swimmer is such that the tumbling condition is given by (4.6), we see that increasingly elongated swimmers (i.e. those with larger B(T)) are always less prone to tumbling than less-elongated swimmers, so long as the flows are such that $E_{11}^*(T)$ and $E_{12}^*(T)$ do not change sign. In other words, the more elongated the swimmer, the more

that tumbling is suppressed in this setting. Further, the period of tumbling $2\pi/q$ increases with elongation in this setting, approaching infinity as we leave this dynamical regime and q approaches zero.

However, this simple conclusion need not hold in more generality. For instance, should $E_{11}^*(T)$ and $E_{12}^*(T)$ change sign over a period, then there is no such guarantee on whether there is an increase or decrease of b^2+c^2 in (4.6) as B(T) increases in magnitude. In particular, such time-dependent details can drive the system into a regime where tumbling is suppressed. This, along with other similarly complicating factors like fast swimmer oscillations, exemplifies and emphasises the more general observation, as also noted in previous studies (Walker *et al.* 2022*a*, 2023), that simply using averaged parameters for flow and swimmer properties can generate fundamentally different and incorrect predictions. Ultimately, this is simply because the operations of averaging and multiplication do not commute.

We also note that (3.13) is a generalised Jeffery equation, describing the angular dynamics of an ellipsoid in a constant planar linear background flow with a self-induced angular velocity $\overline{\Omega}$. Notably, (2.13) still holds for this rigid ellipsoid and simplifies to

$$\frac{d\theta^e}{dt} = \Omega^{*e} + \Omega^e - B^e E_{11}^* \sin 2\theta^e + B^e E_{12}^* \cos 2\theta^e, \tag{4.8}$$

where the superscript e refers to the ellipsoid and its associated constant planar linear flow. Here, B^e corresponds to the Bretherton parameter of the ellipsoid, which we identify with the mean Bretherton parameter of the swimmer, \overline{B} . We can further identify the effective constant flow to be such that

$$\Omega^{*e} = \overline{\Omega}^*, \quad \Omega^e = \overline{\Omega}, \quad a = \Omega^{*e} + \Omega^e = \overline{\Omega}^* + \overline{\Omega}$$
 (4.9)

with, in addition,

$$E_{11}^{*e} = b/B^e = \overline{b}_{\ddagger}/B^e, \quad E_{12}^{*e} = -c/B^e = -\overline{c}_{\ddagger}/B^e.$$
 (4.10)

This ensures that the leading-order angular dynamics of the swimmer is the same as the generalised Jeffery orbit of an ellipsoid with the same mean Bretherton parameter in a constant background flow (that is a complicated function of the original flow and swimmer gait dynamics). Thus, a, b, c may be interpreted as the parameters associated with the generalised Jeffery orbit, with a measuring the contribution of the angular velocity and $(b^2 + c^2)^{1/2}$ measuring the level of shear, weighted by mean swimmer shape parameters. The asymptotic angular behaviour is thereby determined by which of these contributions is dominant.

5. Classification of translational dynamics

From (3.27), we have that the trajectory averaged over the fast oscillations, $\overline{x}_0(t)$, is perturbed by a fast oscillation of zero mean at the leading order of the multiple scales approximation. Furthermore, by inspection of (3.35), any drift in the e_3 direction perpendicular to the plane of the flow can be treated independently once $\tilde{\theta}_0$ is known. In addition, this drift is completely decoupled and only driven by the background flow, unless the swimmer only possesses a D_n , $n \ge 4$ symmetry for part of its gait cycle. In the latter case, shape changes in the body, encapsulated by $\eta_2(T)$, can interact with the strain rate of the flow to generate a non-trivial drift perpendicular to the flow, even in the absence of a background flow component in this direction. In contrast, the dynamics for $\overline{x}_0(t)$ in the plane of flow is much more complex, even for swimmers with high symmetry, which we consider below.

5.1. Exponential temporal dynamics in the plane

If the average strain rate of the flow dominates the average rotation rate of the flow, such that

$$\overline{E_{11}^*}^2 + \overline{E_{12}^*}^2 > \overline{\Omega^*}^2,$$
 (5.1)

then the matrix exponential of (3.45) entails that the swimmer will drift away from its starting point at an exponential rate, irrespective of its angular dynamics and with the possible exception of edge cases. Such edge cases can occur when $\mathbf{K}(t)\overline{\mathbf{x}}_0(t=0)$ is precisely balanced by

$$\int_0^t \mathbf{K}(t-s)\mathbf{C}(\sin 2\tilde{\theta}_0(s), \cos 2\tilde{\theta}_0(s), \sin \tilde{\theta}_0(s), \cos \tilde{\theta}_0(s)) \, \mathrm{d}s. \tag{5.2}$$

However, (5.2) is independent of the initial location of the swimmer. Thus, mathematical precision is required in the initial conditions for such an edge case, which would not be realisable in practice.

5.2. Linear temporal dynamics in the plane

We proceed to consider the degenerate case

$$\overline{E_{11}^*}^2 + \overline{E_{12}^*}^2 = \overline{\Omega^*}^2, \tag{5.3}$$

where $A^2 = 0$ from (3.43). This splits into two further subcases: A = 0 or $A \neq 0$. If A = 0 the flow is either trivial or it is oscillatory with zero mean, so that $E_{++}^* = 0$.

If $\mathbf{A} = \mathbf{0}$, the flow is either trivial or it is oscillatory with zero mean, so that $\overline{E_{11}^*} = \overline{E_{12}^*} = \overline{\Omega^*} = 0$. If the flow is trivial, the equations for translation collapse to

$$\frac{\mathrm{d}\overline{x}_{0}}{\mathrm{d}t} = (V\overline{\cos\Psi} + V_{Uc})\tilde{e}_{10}(\tilde{\theta}_{0}) + (V\overline{\sin\Psi} + V_{Us})\tilde{e}_{20}(\tilde{\theta}_{0})
+ \overline{\Omega I_{Us}}\tilde{e}_{10}(\tilde{\theta}_{0}) - \overline{\Omega I_{Uc}}\tilde{e}_{20}(\tilde{\theta}_{0}),$$
(5.4)

and the swimmer progresses, in general, on a curved trajectory.

For example, even when the swimmer is not rotating on a fast time scale, so that

$$\Omega_f = 0, \quad \Psi = \sin \Psi = I_{Us} = V_{Us} = 0, \quad V_{Uc} = \omega \overline{U} \cos \Psi = \omega \overline{U} = 0$$

$$\tilde{\theta}_0 = \overline{\theta}_0, \quad \tilde{e}_{10}(\tilde{\theta}_0) = \hat{e}_{10}(\overline{\theta}_0), \quad \tilde{e}_{20}(\tilde{\theta}_0) = \hat{e}_{20}(\overline{\theta}_0), \quad (5.5)$$

the equation of motion reduces to

$$\frac{\mathrm{d}\overline{x}_0}{\mathrm{d}t} = V\hat{\boldsymbol{e}}_{10}(\overline{\theta}_0) - \overline{\Omega I_{Uc}}\hat{\boldsymbol{e}}_{20}(\overline{\theta}_0)$$
 (5.6)

and the swimming corresponds to a curved trajectory with radial velocity V and a velocity of $-\overline{\Omega}I_{Uc}$ in the $\overline{\theta}_0$ direction. Moreover, the swimmer trajectory is further modulated by the fast rotation of the swimmer $\Omega_f(T)$ through Ψ , V_{Us} , V_{Uc} , I_{Us} , I_{Uc} , albeit in a much more complex manner than suggested by naive averaging, with $\overline{\Omega}_f = 0$ insufficient to simplify further.

If instead we have $\mathbf{A} = \mathbf{0}$ via a non-trivial mean-zero oscillatory flow, we have $\mathbf{K} = \mathbf{I}$ and

$$\overline{x}_0(t) = \overline{x}_0(t = 0) + \int_0^t C(\sin 2\tilde{\theta}_0(s), \cos 2\tilde{\theta}_0(s), \sin \tilde{\theta}_0(s), \cos \tilde{\theta}_0(s)) \, \mathrm{d}s, \tag{5.7}$$

with C as in (3.47). Suppose that we are in one of the regimes explored in § 4 in which the orientation of the swimmer asymptotes to a fixed value. Then, the integrand of (5.7) becomes constant for large values of the integration variable and, thus, the swimmer will drift to infinity linearly in time (neglecting possible edge cases of perfect cancellation between terms). Notably, this linear drift can happen even if there is only reciprocal swimming, i.e. $V = \overline{\Omega} I_{Us} = \overline{\Omega} I_{Uc} = 0$. This can be seen explicitly in the example setting of fore-aft symmetric swimmers that are a body of revolution, with the equations reducing to those of (C11c) and where $\tilde{\theta}_0 = \overline{\theta}_0$. In this case, contributions to swimming arise from terms such as $\overline{I_{Uc}E_{11}^*}\hat{e}_{10}(\overline{\theta}_0)$, which need not be zero even for reciprocal swimmers. Thus, seemingly non-progressive swimming can generate a drift to spatial infinity through interactions with purely oscillatory, mean-zero flows. In other words, this provides an explicit mechanism by which a swimmer might circumvent Purcell's scallop theorem.

Suppose instead that we are in a regime in which the swimmer tumbles endlessly in the zero-mean oscillatory flow. Note that these flows necessarily have $\overline{\Omega^*} = 0$, so that swimmer tumbling requires $\overline{\Omega}^2 > 0$ in this setting (consider (4.6) with $\overline{\Omega^*} = 0$), thus excluding swimmers with fore-aft symmetry. Proceeding with a swimmer that is tumbling, we can evaluate the contribution of the term associated with $V \overline{\cos \Psi}$ in the inertial frame e_1 direction in (5.7) over a single period of rotation. For one such tumble, which we recall has period $2\pi/q$, starting from some $t = t_s$, this contribution is $V \overline{\cos \Psi}$ multiplied by

$$\int_{t_s}^{t_s+2\pi/q} \cos\tilde{\theta}_0 dt = \int_{\tilde{\theta}_0(t_s)}^{\tilde{\theta}_0(t_s)+2\pi} \frac{\cos\tilde{\theta}_0}{a-b\sin 2\tilde{\theta}_0 - c\cos 2\tilde{\theta}_0} d\tilde{\theta}_0$$

$$= \frac{1}{a} \int_{-\pi}^{\pi} \frac{\cos\tilde{\theta}_0}{1-R\cos(2\tilde{\theta}_0 - 2\xi)} d\tilde{\theta}_0, \text{ with } R = \frac{(b^2+c^2)^{1/2}}{a} < 1, \qquad (5.8)$$

where ξ is a phase shift. Here, we have recalled the governing equation of (3.13) to change variables to $\tilde{\theta}_0$ in the integrals. Using the periodicity of the cosines, this can be written as a linear combination of the following integrals:

$$\frac{1}{a} \int_{-\pi}^{\pi} \frac{\cos\tilde{\theta}_0}{1 - R\cos(2\tilde{\theta}_0)} d\tilde{\theta}_0 = \frac{2}{a} \int_0^{\pi} \frac{\cos\tilde{\theta}_0}{1 - R\cos(2\tilde{\theta}_0)} d\tilde{\theta}_0, \quad \frac{1}{a} \int_{-\pi}^{\pi} \frac{\sin\tilde{\theta}_0}{1 - R\cos(2\tilde{\theta}_0)} d\tilde{\theta}_0.$$
(5.9)

Both of these integrals are zero, by the odd parity in reflection about $\theta_0 = \pi/2$ for the first integral and about $\theta_0 = 0$ for the second. Similarly, all other terms contributing to the translational motility in (5.7) can be written as a linear combination of integrals over a temporal period, with integrands

$$\sin \theta_0$$
, $\sin 2\theta_0 \cos \theta_0$, $\cos 2\theta_0 \cos \theta_0$, $\sin 2\theta_0 \sin \theta_0$, $\cos 2\theta_0 \sin \theta_0$, (5.10)

which all integrate to zero using the same arguments as above. Hence, we may conclude that a tumbling swimmer in a purely oscillatory linear planar flow does not drift indefinitely.

Now we consider the final subcase of linear temporal dynamics in the plane, assuming that $\mathbf{A} \neq \mathbf{0}$ and $\mathbf{A}^2 = \mathbf{0}$. We consider the Jordan normal form for \mathbf{A} to within an overall scaling, though it is also useful to explicitly demonstrate that the transformation required in this particular case is a rotation. First, let e_A denote the zero-eigenvalue unit eigenvector of \mathbf{A} (unique up to sign) and, thus, $\mathbf{A}e_A = \mathbf{0}$. Additionally, let e_A^{\perp} denote the unit vector

perpendicular to e_A so that $\{e_A, e_A^{\perp}\}$ is a right-handed orthonormal basis. We have $\mathbf{A}e_A^{\perp} \neq \mathbf{0}$, otherwise $\mathbf{A} = \mathbf{0}$. Then, with α_1 and α_2 defined by

$$\mathbf{A}\mathbf{e}_{A}^{\perp} = \alpha_{1}\mathbf{e}_{A} + \alpha_{2}\mathbf{e}_{A}^{\perp} \tag{5.11}$$

we have $\mathbf{0} = \mathbf{A}^2 \mathbf{e}_A^{\perp} = \alpha_2 \mathbf{A} \mathbf{e}_A^{\perp}$ and, hence, $\alpha_2 = 0$ and $\alpha_1 \neq 0$. Thus,

$$\mathbf{A} \left[\mathbf{e}_A | \mathbf{e}_A^{\perp} \right] = \left[\mathbf{0} | \alpha_1 \mathbf{e}_A \right] = \left[\mathbf{e}_A | \mathbf{e}_A^{\perp} \right] \begin{bmatrix} 0 & \alpha_1 \\ 0 & 0 \end{bmatrix}. \tag{5.12}$$

Noting that $[e_A|e_A^{\perp}]$ is an orthogonal matrix, using its transpose to left-multiply both sides shows that a rotation of the axes can be found to transform $\bf A$ to a matrix that is zero except for the upper right-hand off-diagonal entry (this is the Jordan normal form of $\bf A$ to within scaling). Hence, the flows we are considering here are, on averaging, those of pure shear with $\overline{u^*} = 2\overline{E_{12}^*}ye_1$ for a suitable choice of orthonormal basis, and we have $\overline{E_{12}^*} \neq 0$ as $\bf A \neq 0$.

For swimmers that asymptote to a fixed angle, the presence of pure shear results in infinite drift in the e_1 direction, parallel to the flow, that increases quadratically in time in general. This arises from the fact that the dominant term in the e_1 direction for $t \gg t_* \gg 1$ (sufficiently large) is approximately

$$\begin{bmatrix}
\int_{t_{*}}^{t} \mathbf{I} + \mathbf{A}(t - s) \, \mathrm{d}s
\end{bmatrix} \mathbf{C}(\sin 2\tilde{\theta}_{0}, \cos 2\tilde{\theta}_{0}, \sin \tilde{\theta}_{0}, \cos \tilde{\theta}_{0})\Big|_{\tilde{\theta}_{0} = \tilde{\theta}_{0}(\infty)}$$

$$= \begin{bmatrix}
\int_{t_{*}}^{t} \begin{bmatrix} 1 & 2\overline{E_{12}^{*}}(t - s) \\ 0 & 1 \end{bmatrix} \, \mathrm{d}s
\end{bmatrix} \mathbf{C}(\sin 2\tilde{\theta}_{0}, \cos 2\tilde{\theta}_{0}, \sin \tilde{\theta}_{0}, \cos \tilde{\theta}_{0})\Big|_{\tilde{\theta}_{0} = \tilde{\theta}_{0}(\infty)}$$

$$\sim \begin{bmatrix} \operatorname{ord}(t^{2}) \\ \operatorname{ord}(t) \end{bmatrix}. \tag{5.13}$$

Finally, we note that a tumbling swimmer's trajectory will drift in the e_1 direction in all but edge cases due to the

$$\mathbf{K}(t)\overline{\mathbf{x}}_0(t=0) = (\mathbf{I} + \mathbf{A}t)\overline{\mathbf{x}}_0(t=0)$$
(5.14)

term. However, it will not drift in the e_2 direction. In particular, given the swimmer is tumbling and noting $e_2^{\top} A = 0$, we have that its location in the e_2 direction is given by

$$\begin{aligned} \boldsymbol{e}_{2}^{\top} \overline{\boldsymbol{x}}_{0}(t) &= \boldsymbol{e}_{2}^{\top} \overline{\boldsymbol{x}}_{0}(t=0) \\ &+ \boldsymbol{e}_{2}^{\top} \int_{0}^{t} (\boldsymbol{I} + \boldsymbol{A}(t-s)) \boldsymbol{C}(\sin 2\tilde{\theta}_{0}(s), \cos 2\tilde{\theta}_{0}(s), \sin \tilde{\theta}_{0}(s), \cos \tilde{\theta}_{0}(s)) \, \mathrm{d}s, \\ &= \boldsymbol{e}_{2}^{\top} \overline{\boldsymbol{x}}_{0}(t=0) + \int_{0}^{t} \boldsymbol{e}_{2}^{\top} \boldsymbol{C}(\sin 2\tilde{\theta}_{0}(s), \cos 2\tilde{\theta}_{0}(s), \sin \tilde{\theta}_{0}(s), \cos \tilde{\theta}_{0}(s)) \, \mathrm{d}s. \end{aligned} \tag{5.15b}$$

The integral above is the second component of those occurring in (5.7) for a tumbling swimmer, as considered in (5.8) and (5.9), and, thus, by an inheritance of this analysis we can deduce that there is no drift in the e_2 direction for a tumbling swimmer in a flow that is pure shear and non-trivial after time averaging.

5.3. Oscillatory temporal dynamics in the plane

The final class of translational dynamics to consider occurs if the average strain rate is dominated by the rotation rate, such that

$$\overline{E_{11}^*}^2 + \overline{E_{12}^*}^2 < \overline{\Omega^*}^2. \tag{5.16}$$

Neglecting edge cases, we first consider swimming in which $a^2 < b^2 + c^2$, so that there is no tumbling and, hence, the swimmer tends to a fixed angle for large time (see § 4). Noting from (3.45) that K(t) is periodic on the slow time scale with period $2\pi/\mu$, where

$$\mu = (\overline{\Omega^*}^2 - \overline{E_{11}^*}^2 - \overline{E_{12}^*}^2)^{1/2},\tag{5.17}$$

we have for t_* sufficiently large

$$\overline{\mathbf{x}}_{0}(t_{*}+2\pi/\mu)-\overline{\mathbf{x}}_{0}(t_{*})$$

$$\approx \left[\int_{t_{*}}^{t_{*}+2\pi/\mu}\mathbf{K}(t_{*}-s)\,\mathrm{d}s\right]\mathbf{C}(\sin 2\tilde{\theta}_{0},\cos 2\tilde{\theta}_{0},\sin \tilde{\theta}_{0},\cos \tilde{\theta}_{0})\Big|_{\tilde{\theta}_{0}=\tilde{\theta}_{0}(\infty)}=0. \quad (5.18)$$

The error in approximating θ_0 by its asymptote is exponentially small for large time (see (3.16)) and, hence, these errors do not accumulate. Thus, the trajectory is asymptotically periodic and bounded for large time. Furthermore, even with net motion of the swimmer, so that at least one of V, ΩI_{Uc} or ΩI_{Us} is not zero, the contribution of the progressive swimming to the motion for $t > t_*$ (with t_* sufficiently large) is zero. For example, when V > 0, the contribution to the motion for $t > t_*$ that scales with $V \cos \Psi$ is (to within exponentially small errors) given by

$$V\overline{\cos\Psi} \left[\int_0^t \mathbf{K}(t-s) \, \mathrm{d}s - \int_0^{t_*} \mathbf{K}(t_*-s) \, \mathrm{d}s \right] \hat{\mathbf{e}}_{10}(\infty)$$

$$= V\overline{\cos\Psi} \left(\frac{\sin(\mu t_*) - \sin(\mu t)}{\mu} + \frac{\cos(\mu t) - \cos(\mu t_*)}{\mu^2} \mathbf{A} \right) \hat{\mathbf{e}}_{10}(\infty), \tag{5.19}$$

with K as in (3.45). In particular, this contribution is oscillatory as t increases. Directly analogous and oscillatory results also hold for all terms involving

$$V, V_{Uc}, V_{Us}, \overline{\Omega I_{Uc}}, \overline{\Omega I_{Us}}.$$
 (5.20)

In turn, this explicitly demonstrates that the progressive movement of the swimmer has been converted to an oscillatory movement by the background flow.

In contrast, if the tumbling condition holds, that is $a^2 > b^2 + c^2$, the dynamics will involve the convolution of oscillations at the tumbling frequency and at the frequency associated with the flow

$$\mu = (\overline{\Omega^*}^2 - \overline{E_{11}^*}^2 - \overline{E_{12}^*}^2)^{1/2}.$$
 (5.21)

Whether such dynamics induces oscillations or unbounded dynamics in the trajectory at long time is contingent on whether or not there is resonance between the different oscillatory contributions, though oscillations may be typically expected as resonance requires parameter fine-tuning. Though general results in this case are less forthcoming, we can examine special cases of (3.16) and (3.46) to yield additional insights, as we pursue below.

6. Bodies of revolution with fore-aft symmetry

While the analytical cases above considered relatively general bodies, emphasising the ubiquity of the observations among different body shapes, the special cases below are restricted to bodies of revolution that possess fore-aft symmetry, unless explicitly stated otherwise. Hence, only $-\lambda_2(T) \equiv B(T)$, the Bretherton parameter, is non-zero for the interactions between the rate of strain and the swimmer dynamics in (2.17). In addition, fore-aft symmetry implies that $\Omega_f = \Omega = 0$ and, hence, $\Psi = \sin \Psi = 0$, giving the simplifications of (5.5).

With these restrictions and simplifications, the angular dynamics are given by (3.16) with the additional reductions

$$a_{\dagger} = \Omega^*, \quad b_{\dagger} = b_{\ddagger} = B E_{11}^* \quad c_{\dagger} = c_{\ddagger} = -B E_{12}^*,$$
 (6.1)

which arise from (3.1) and (3.10). For both clarity and the interested reader, the equations of motion are explicitly simplified in Appendix C, where we have from (C11) that motion in the e_3 direction is trivial. The translational equation of motion in the flow plane reduces to

$$\frac{d\overline{x}_{0}}{dt} = \underbrace{\begin{bmatrix} \overline{E}_{11}^{*} & \overline{E}_{12}^{*} - \overline{\Omega}^{*} \\ \overline{E}_{12}^{*} + \overline{\Omega}^{*} & -\overline{E}_{11}^{*} \end{bmatrix}}_{\boldsymbol{A}} \overline{x}_{0} + \begin{bmatrix} V + \overline{I_{Uc}E_{11}^{*}} & \overline{I_{Uc}E_{12}^{*}} \\ \overline{I_{Uc}E_{12}^{*}} & V - \overline{I_{Uc}E_{11}^{*}} \end{bmatrix} \hat{\boldsymbol{e}}_{10}(\overline{\theta}_{0}) + \left(\overline{I_{Uc}BE_{11}^{*}} \sin 2\overline{\theta}_{0} - \overline{I_{Uc}BE_{12}^{*}} \cos 2\overline{\theta}_{0} \right) \hat{\boldsymbol{e}}_{20}(\overline{\theta}_{0}), \tag{6.2}$$

and we have dropped the constant background flow contribution, \overline{u}_{tr}^* , without loss of generality by the choice of inertial reference frame.

In this reduced yet still complex setting, we will explore swimmer behaviours in various planar linear flows and demonstrate that simple dynamics emerge despite the level of complexity remaining.

6.1. Rotational flow

A particularly simple case is that of rotational flow with non-zero mean, for which $E_{11}^*=E_{12}^*=0$ and $\overline{\Omega^*}\neq 0$. In this regime, the tumbling condition of § 4 holds, with $a=\overline{\Omega^*}\neq 0$ and b=c=0, so that (3.16) reduces to

$$\overline{\theta}_0 = \theta_{00} + \overline{\Omega^*}t, \tag{6.3}$$

where $\theta_{00} = \overline{\theta}_0(t=0)$. Further, with $\overline{x}_0 = e_1 \cdot \overline{x}_0$, $\overline{y}_0 = e_2 \cdot \overline{x}_0$, we have

$$\frac{d\overline{x}_0}{dt} = -\overline{\Omega}^* \overline{y}_0 + V \cos \overline{\theta}_0, \quad \frac{d\overline{y}_0}{dt} = \overline{\Omega}^* \overline{x}_0 + V \sin \overline{\theta}_0. \tag{6.4}$$

Hence, if there is no intrinsic net swimming (V = 0), the overall motion is that of simple harmonic oscillations, with

$$\frac{\mathrm{d}^2 \overline{x}_0}{\mathrm{d}t^2} + \overline{\Omega}^{*2} \overline{x}_0 = 0 \tag{6.5}$$

and, thus, there is no net motion on the long time scale for non-progressive swimmers with this level of symmetry in purely rotational flow.

For $V \neq 0$, we instead have the dynamics of a forced oscillator, with

$$\frac{\mathrm{d}^2 \overline{x}_0}{\mathrm{d}t^2} + \overline{\Omega^*}^2 \overline{x}_0 = -2V \overline{\Omega^*} \sin\left(\theta_{00} + \overline{\Omega^*}t\right), \quad \overline{y}_0 = \frac{1}{\overline{\Omega^*}} \left[V \cos\overline{\theta}_0 - \frac{\mathrm{d}\overline{x}_0}{\mathrm{d}t}\right], \quad (6.6)$$

which generates resonance with no parameter fine-tuning beyond that needed to force a purely rotational flow. Thus, for purely rotational flow and even slightly progressive swimmers, we conclude that swimmer motility generates a resonant oscillation, so that the swimmer distance from the origin scales linearly with time. Recovering additional generality by reinstating the shape parameters λ_5 , η_2 , η_3 and η_4 does not change these observations, as they enter the equations of motion through the rate of strain tensor, which here is zero.

However, if we relax the constraint of fore—aft symmetry and allow the swimmer to generate a slow time scale rotation $\Omega \neq 0$, then $a = \overline{\Omega} + \overline{\Omega^*} \neq \overline{\Omega^*}$. In turn, (6.3) no longer holds and the corresponding forcing in (6.6) is modified to a term scaling with $\sin(\theta_{00} + at)$. Thus, the swimmer oscillates and resonance does not occur, demonstrating that an element of fine tuning (i.e. perfect fore—aft symmetry) is indeed required for resonance.

6.2. Irrotational flow

For an irrotational flow with non-trivial mean, we have $\Omega^*=0$, $\overline{E_{11}^*}^2+\overline{E_{12}^*}^2>0$. Recalling $\Omega=0$ by fore-aft symmetry, we also have a=0 and, by (3.16), $\overline{\theta}_0$ tends to a constant asymptote for large time. From (5.1) *et seq.*, we have exponential dynamics in the plane and, recognising the possible exception of edge cases, the swimmer drifts off to spatial infinity. This long-time trajectory can be examined in more detail without further loss of generality. As $\Omega^*=0$, the matrix $\bf A$ of (6.2) is symmetric and, hence, diagonalisable. Thus, with a suitable choice of laboratory basis, the equations of motion in the plane of the flow in the long-time limit are given approximately by

$$\frac{d\overline{x}_0}{dt} = \left(\overline{E_{11}^*}^2 + \overline{E_{12}^*}^2\right)^{1/2} (\overline{x}_0 + \alpha), \quad \frac{d\overline{y}_0}{dt} = -\left(\overline{E_{11}^*}^2 + \overline{E_{12}^*}^2\right)^{1/2} (\overline{y}_0 + \beta), \quad (6.7)$$

where

$$\alpha \left(\overline{E_{11}^*}^2 + \overline{E_{12}^*}^2\right)^{1/2}, \quad -\beta \left(\overline{E_{11}^*}^2 + \overline{E_{12}^*}^2\right)^{1/2}$$
 (6.8)

are the first and second components of the long-time limits of the other terms in (6.2). Noting the opposing signs of the eigenvalues in (6.7), this explicitly demonstrates an exponential drift to infinity in one direction accompanied by an exponential decay towards a constant in the orthogonal direction. Further, we have

$$\frac{\mathrm{d}\overline{y}_0}{\mathrm{d}\overline{x}_0} = -\frac{\overline{y}_0 + \beta}{\overline{x}_0 + \alpha} \tag{6.9}$$

and, hence,

$$\overline{y}_0 + \beta = \frac{M}{\overline{x}_0 + \alpha},\tag{6.10}$$

where M is a constant of integration. Thus, independent of any further details, a swimmer in such an irrotational flow moves along hyperbolae in the plane once initial transients have decayed. Furthermore, noting the change of basis to bring the equation of motion into the form of (6.7), the hyperbola asymptote is parallel to an eigenvector of the averaged rate of strain tensor, \overline{E}^* . We showcase an example of asymptoting towards a hyperbola in figure 2, and note that the long-time direction of motion of this swimmer is given by an eigenvector of \overline{E}^* , in this case $[(1 + \sqrt{5})/2, 1]^{\top}$.

Notably, these broad conclusions apply for both progressive and non-progressive swimmers. They also apply if we relax many of our symmetry constraints (with the exception of fore–aft reflection invariance), with these results holding for non-zero η_2 , η_3 , η_4 and λ_5 . The breaking of fore–aft symmetry, however, allows for self-induced rotation

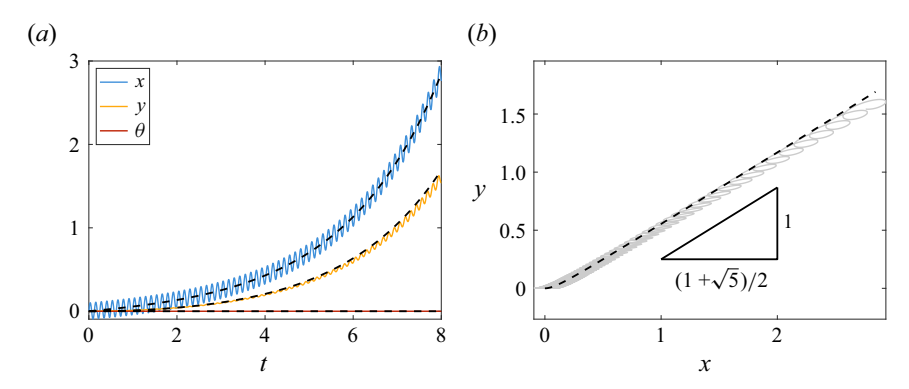


Figure 2. Exponential translational dynamics of a swimmer in irrotational oscillatory flow. (a) The temporal evolution of swimmer position and orientation, highlighting long-time exponential growth of x and y and a constant-average orientation θ . (b) The path of the swimmer from (x,y)=(0,0) is shown in grey, which exhibits large oscillations around an eventually hyperbolic trajectory. This hyperbola asymptotes to a line with gradient $2/(1+\sqrt{5})$, parallel to an eigenvector of the averaged rate of strain tensor $\overline{E^*}$. The leading-order approximations to the average evolution are shown as black dashed lines, evidencing excellent agreement with the full numerical solutions that expectedly lessens during the exponential translational motion. Here, we have taken $\omega=100$ and set all swimmer and flow parameters to be zero apart from $U(T)=0.1\cos T$, $E_{11}^*(T)=0.2+\sin T$ and $E_{12}^*(T)=0.4+\sin T$.

that has the potential to invalidate these conclusions, as we plausibly obtain a > 0 and lose the asymptoting behaviour of the swimmer orientation.

6.3. Motility in stationary shear

The classical example of a stationary shear flow can be recovered by setting $E_{11}^*=0$ and $\Omega^*=-E_{12}^*\neq 0$ and constant, without loss of generality. In this case, (3.16) and (3.46) entail that \bar{y}_0 and $\bar{\theta}_0$ decouple from \bar{x}_0 , with motion in the latter direction including an inexorable drift in all but edge cases. Hence, we focus on the dynamics of \bar{y}_0 and $\bar{\theta}_0$, which here are governed by the reduced system

$$\frac{\mathrm{d}\bar{y}_0}{\mathrm{d}t} = -E_{12}^* \overline{I_{Uc}B} \cos \bar{\theta}_0 \cos 2\bar{\theta}_0 + V \sin \bar{\theta}_0, \tag{6.11a}$$

$$\frac{\mathrm{d}\bar{\theta}_0}{\mathrm{d}t} = -E_{12}^* \left(1 - \overline{B}\cos 2\bar{\theta}_0 \right),\tag{6.11b}$$

recalling that $\overline{I_{Uc}} = 0$.

We first consider the case with $|\overline{B}| < 1$. Equation (6.11*b*) immediately implies that $\bar{\theta}_0$ is periodic, which can also be seen in the general formalism of (3.13) and (3.16) by setting $a = -E_{12}^*$, b = 0, $c = -E_{12}^*\overline{B}$ and $q = (a^2 - b^2 - c^2)^{1/2} = |E_{12}^*|(1 - \overline{B}^2)^{1/2} > 0$. This dynamics corresponds precisely to that of planar Jeffery orbits (Jeffery 1922), as generalised by Bretherton (1962) and identified in planar shape-changing swimmers by Gaffney *et al.* (2022*a*).

We also have that \bar{y}_0 is periodic, as can be deduced by observing that the system is conservative, with

$$\frac{\mathrm{d}H}{\mathrm{d}t} = 0, \quad H := \bar{y}_0 - \int_0^{\bar{\theta}_0} \frac{1}{1 - \overline{B}\cos 2\psi} \left(\overline{I_{Uc}B}\cos\psi\cos 2\psi - \frac{V}{E_{12}^*}\sin\psi \right) \mathrm{d}\psi. \tag{6.12}$$

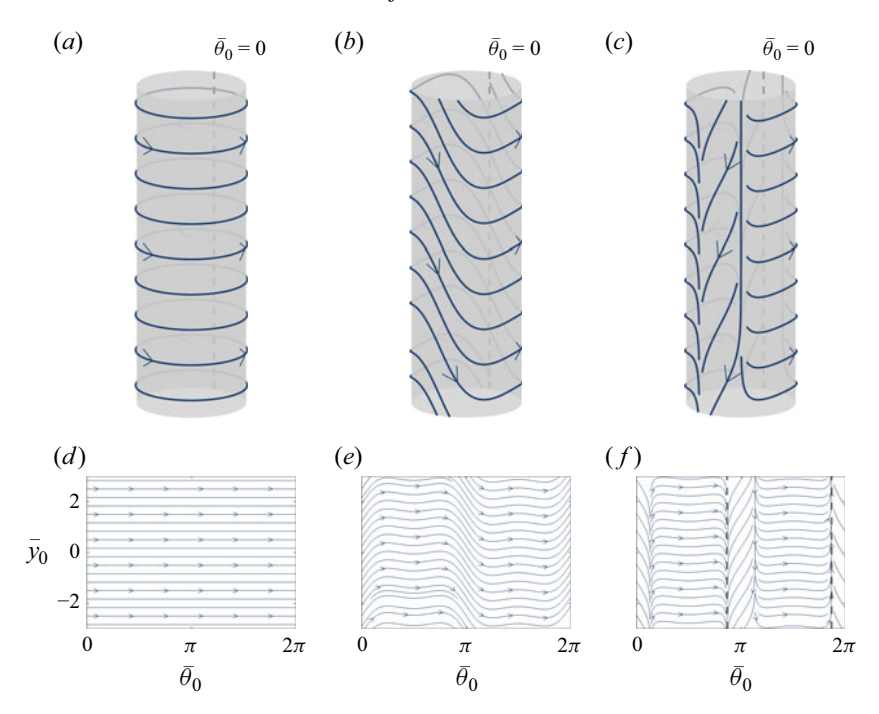


Figure 3. Systematically averaged dynamics of a reciprocal swimmer in stationary shear flow, a scenario schematically illustrated in figure 1 with a depiction of θ , y. In the above, note that $\overline{\theta_0}$, $\overline{y_0}$ are the fast time scale averages of the leading-order approximations, that is θ_0 , y_0 , to the variables θ , y. In the above, we illustrate the semiperiodic phase space that corresponds to a reciprocal swimmer in stationary shear flow, shown both as dynamics on a cylinder and in the plane. We showcase three qualitatively distinct regimes: in (a) and (d), we have $(\overline{I_{Uc}B}, \overline{B}) = (0, 0.5)$, leading to no motion at leading order; in (b) and (e), we have $(\overline{I_{Uc}B}, \overline{B}) = (1, 0.5)$ and long-time periodic motion; in (c) and (f), we have $(\overline{I_{Uc}B}, \overline{B}) = (1, 1.5)$ and progression. In (f), the dashed lines correspond to stable states of the angular dynamics.

Thus, as H is constant, we have that \bar{y}_0 is an integral of a smooth, bounded integrand with periodic limits, up to an additive constant. Hence, \bar{y}_0 is bounded and periodic for all time. It inherits the period of $\bar{\theta}_0$, which here is given by

$$\frac{2\pi}{q} = \frac{2\pi}{(a^2 - c^2)^{1/2}} = \frac{2\pi}{|E_{12}^*|(1 - \overline{B}^2)^{1/2}}$$
(6.13)

in units of the slow time scale.

Now suppose that $|B| \geqslant 1$, a case that requires extreme shape elongation (Bretherton 1962). This gives rise to fundamentally different dynamics, with the swimmer no longer tumbling. Instead, its angle asymptotes to a constant that, in turn, induces a drift to infinity along the e_2 direction (perpendicular to the flow direction) for large time. This is even true for reciprocal swimmers if $\overline{I_{Uc}B} \neq 0$. In other words, it is possible for a highly elongated reciprocal swimmer with fore—aft symmetry to self-propel indefinitely across pathlines in a stationary shear flow via the interaction between shear flow and the swimmer deformation.

The range of possible leading-order dynamics for a reciprocal swimmer (V=0) in various flows is illustrated in figure 3, with figure 3(b,e) showcasing periodicity on a long time scale Jeffery orbit. Non-trivial motility is highlighted in figure 3(c,f), in which the reciprocal swimmer approaches a steady state of the angular dynamics and achieves net propulsion across pathlines of the flow.

E.A. Gaffney, K. Ishimoto and B.J. Walker

6.4. Motility in oscillatory shear

A natural generalisation of stationary shear flow is oscillatory shear flow. For such a flow, we have $E_{11}^* = 0$ and $\Omega^*(T) = -E_{12}^*(T) \neq 0$, without loss of generality. The equations of motion simplify to

$$\frac{\mathrm{d}\overline{x}_0}{\mathrm{d}t} = 2\overline{E}_{12}^* \overline{y}_0 + \overline{E}_{12}^* I_{Uc} \sin \overline{\theta}_0 + \overline{E}_{12}^* I_{Uc} B \sin \overline{\theta}_0 \cos 2\overline{\theta}_0 + V \cos \overline{\theta}_0, \tag{6.14a}$$

$$\frac{\mathrm{d}\bar{y}_0}{\mathrm{d}t} = \overline{E_{12}^* I_{Uc}} \cos \bar{\theta}_0 - \overline{E_{12}^* I_{Uc} B} \cos \bar{\theta}_0 \cos 2\bar{\theta}_0 + V \sin \bar{\theta}_0, \tag{6.14b}$$

$$\frac{\mathrm{d}\bar{\theta}_0}{\mathrm{d}t} = -\overline{E}_{12}^* \left(1 - \frac{\overline{E}_{12}^* B}{\overline{E}_{12}^*} \cos 2\bar{\theta}_0 \right),\tag{6.14c}$$

noting the appearance of an effective Bretherton parameter of $\overline{E_{12}^*B}/\overline{E_{12}^*}$ in (6.14c). Importantly, this quantity need not have magnitude less than unity, even if |B(T)| < 1 for all T. Here, one could replace E_{12}^* with the usual simple shear rate γ via the relation $\gamma(T) := -2E_{12}^*(T)$, corresponding to $u^* = -\gamma(T)ye_1$, though we do not do so here.

Below, we only consider cases where the effective Bretherton parameter has a magnitude greater than unity, noting that this does not necessitate the geometrical constraint of severe elongation, though it does mean the angular dynamics is asymptoting. In this case, the angular dynamics evolves to an asymptotically constant angle at large time. This holds even if the average shear rate is zero (i.e. $\overline{E_{12}^*} = 0$) but $\overline{E_{12}^*B} \neq 0$, in which case we instead have

$$\frac{\mathrm{d}\bar{\theta}_0}{\mathrm{d}t} = \overline{E_{12}^* B} \cos 2\bar{\theta}_0 \tag{6.15}$$

and the angular dynamics evolves to an asymptotic state with $\cos 2\bar{\theta}_0 = 0$.

For the moment, we assume that $\overline{E_{12}^*} \neq 0$ and define $\mathcal{C} = \overline{E_{12}^*}/\overline{E_{12}^*B} \in [-1,1]$ as the reciprocal of the effective Bretherton parameter, the long-time asymptote for $\cos 2\bar{\theta}_0$. We also assume that the long time asymptote is a stable equilibrium and, thus, exclude edge cases of an initial condition at an unstable equilibrium for $\bar{\theta}_0$. We then have that the long-time asymptote for $\bar{\theta}_0$ is either in the interval $\bar{\theta}_0 \in (0, \pi/2)$ or the interval $\bar{\theta}_0 \in (\pi, 3\pi/2)$ and, thus, the signs of $\sin \bar{\theta}_0$ and $\cos \bar{\theta}_0$ are the same for the long-time asymptote. With this, we have

$$\mathcal{A} := \left. (\overline{E_{12}^* I_{Uc}} \sin \overline{\theta}_0 + \overline{E_{12}^* I_{Uc} B} \sin \overline{\theta}_0 \cos 2\overline{\theta}_0 + V \cos \overline{\theta}_0) \right|_{\cos 2\overline{\theta}_0 = \mathcal{C}} \tag{6.16a}$$

$$= \pm \left[\frac{\sqrt{1-\mathcal{C}}}{\sqrt{2}} \left(\overline{E_{12}^* I_{Uc}} + \overline{E_{12}^* I_{Uc} B} \mathcal{C} \right) + \frac{V\sqrt{1+\mathcal{C}}}{\sqrt{2}} \right], \tag{6.16b}$$

$$\mathcal{B} := \left(\overline{E_{12}^* I_{Uc}} \cos \bar{\theta}_0 - \overline{E_{12}^* I_{Uc} B} \cos \bar{\theta}_0 \cos 2\bar{\theta}_0 + V \sin \bar{\theta}_0 \right) \Big|_{\cos 2\bar{\theta}_0 = \mathcal{C}}$$
(6.16c)

$$=\pm\left[\frac{\sqrt{1+\mathcal{C}}}{\sqrt{2}}\left(\overline{E_{12}^*I_{Uc}}-\overline{E_{12}^*I_{Uc}B}\mathcal{C}\right)+\frac{V\sqrt{1-\mathcal{C}}}{\sqrt{2}}\right].$$
(6.16*d*)

In turn, for large time, we have

$$\frac{\mathrm{d}\overline{y}_0}{\mathrm{d}\overline{x}_0} \approx \frac{\mathcal{B}}{\mathcal{A} + 2\overline{E}_{12}^* \overline{y}_0}.$$
(6.17)

Neglecting the asymptotically small errors in this approximation, one may integrate to give

$$\mathcal{B}\overline{x}_0 = \mathcal{K} + \mathcal{A}\overline{y}_0 + \overline{E_{12}^*}\overline{y}_0^2, \tag{6.18}$$

where K is a constant. Thus, excluding possible edge cases, the long-time swimmer trajectories are parabolic, regardless of the details of the flow and the swimming. One such edge case is B = 0, which gives the limiting case of a line of constant \overline{y}_0 , for instance.

Finally, for the case where there is no net shear, we have $\overline{E_{12}^*} = 0$ and assume that $\overline{E_{12}^*B} \neq 0$. Here, the trajectory is also linear, even though naive averaging would predict that the reciprocal swimmer has no net motion. In particular, we have $\mathcal{C} = 0$ and $\mathcal{A} = \mathcal{B}$, regardless of whether V = 0 or $V \neq 0$. Then we have

$$\frac{\mathrm{d}\overline{y}_0}{\mathrm{d}\overline{x}_0} \approx 1,\tag{6.19}$$

so that the trajectories are simply straight lines of unit gradient, independent of the details of the flow, swimmer and initial conditions, at least once the angular dynamics is asymptoting. Example such trajectories are shown for reciprocal swimmers in figure 4(b), with the associated angular dynamics illustrated in figure 4(c). This highlights two explicit examples of reciprocal swimmers in a zero-mean oscillating shear swimming across pathlines, breaking Purcell's scallop theorem. Notably, extensive swimmer elongation is not required to be in this dynamical regime.

7. Discussion and conclusions

We have considered swimmers that are characterised by a separation of time scales, with motility driven by fast time scale processes such as swimmer treadmilling and shape changes. These drivers are independent of the background flow and induce motility associated with a slower time scale, as frequently observed (Smith *et al.* 2009; Curtis & Gaffney 2013; Ishimoto & Gaffney 2014; Pak & Lauga 2015). The swimmer may also induce its own rotation on the fast time scale, though we have assumed a degree of symmetry throughout the motion. In particular, the swimmer is assumed to possess helicoidal symmetry together with additional symmetries associated with reflection planes or rotation axes. These symmetries are summarised in § 2.2, with the simplest case corresponding to a body of revolution and fore—aft symmetry.

Within this framework, we have derived the equations of motion for both the swimmer translational and angular motility, making use of multiscale asymptotic methods that exploit the ratio of time scales to generate simplified equations for the leading-order dynamics on the slow time scale. As expected, given the restrictions imposed on the swimmer, any motion perpendicular to the plane of the flow decouples and we essentially neglect this trivial aspect of the flow. The angular dynamics and the planar translation dynamics are given by a rapid periodic oscillation induced by the swimmer activity, superimposed with angular changes and trajectories that evolve on the slow time scale.

The full system of governing equations is intricate, involving the large number of variables and parameters summarised in tables 1 and 2. In analysing the slow dynamics, however, it is clear that the resulting motion can be extensively characterised by only two groups of variables, whose roles we have identified systematically. These are

$$W_{rot} := \frac{a^2}{b^2 + c^2}$$
 and $W_{trans} := \frac{\overline{\Omega^*}^2}{\overline{E_{11}^*}^2 + \overline{E_{12}^*}^2},$ (7.1)

E.A. Gaffney, K. Ishimoto and B.J. Walker

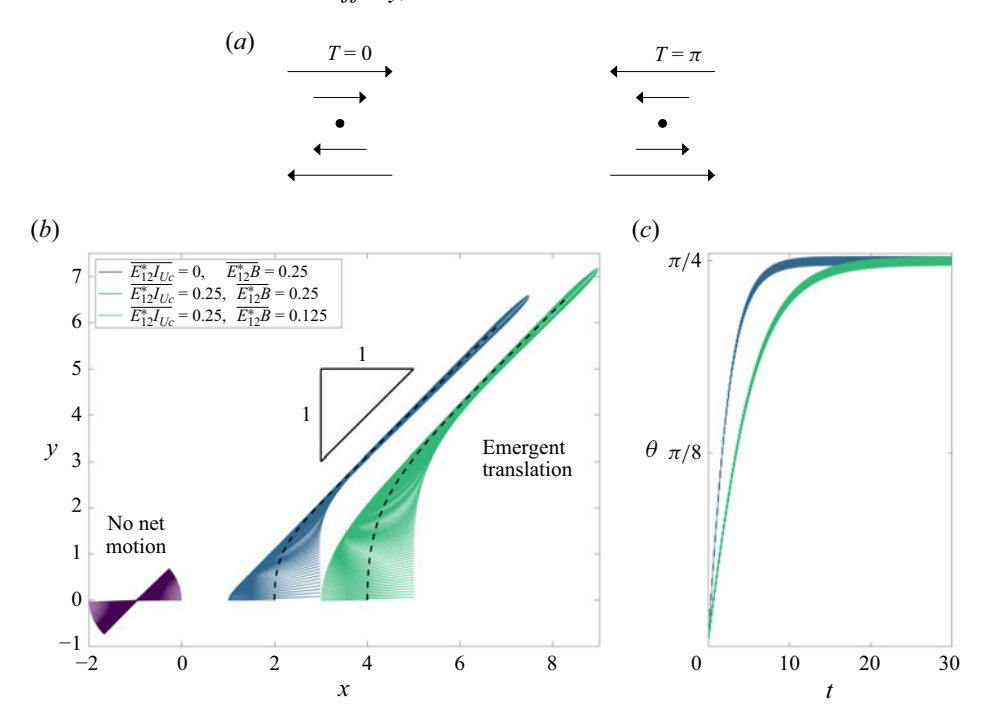


Figure 4. Behaviours of reciprocal swimmers (V=0) in unsteady shear flow with zero average shear. (a) An illustration of the oscillatory flow field. (b) Swimmer trajectories within the oscillatory shear, with the associated angular dynamics and parameters shown in (c). The fast time scale oscillations are clearly visible, as well as the emergent long time behaviours, which can include net motion across pathlines despite reciprocal swimming. The numerical solution of the effective governing equations of (6.14) is shown for two parameter sets as black dashed curves, demonstrating excellent agreement with the average behaviour of the full system. In all cases, the orientation θ asymptotes to a root of $\cos 2\theta_0$, here $\pi/4$, and the gradient of the swimmer trajectory asymptotes to unity, as predicted by the asymptotic analysis. Note that only two curves are visible in (c), as two parameter sets have identical averaged angular dynamics. These are universal predictions for swimmers with sufficient symmetry (such as maintaining a shape that is always a body of revolution with fore–aft symmetry).

which describe the swimming activity and the background flow in turn. Here, a is the fast time scale average of the angular velocity of the swimmer and the background flow, while b^2+c^2 measures the impact of the fast time scale average of the fluid rate of strain on the swimmer's angular dynamics. Similarly, $\overline{\Omega^*}$ is the fluid angular velocity and $(\overline{E_{11}^*}^2+\overline{E_{12}^*}^2)^{1/2}$ is a measure of the rate of strain, both averaged over the fast time scale. Hence, the behaviour of the system is characterised by whether or not angular velocity dominates the impact of rate of strain for both the swimmer and the fluid.

We graphically summarise the key roles of these effective parameters in figure 5, highlighting a markedly simple classification of the long-time dynamics (excluding edge cases). Note that the angular dynamics conditionally reduces to that of a generalised planar Jeffery orbit, linking the angular dynamics to previous investigations, especially Jeffery (1922) and Bretherton (1962). In particular, whether the swimmer asymptotes to a fixed angle of swimming or endlessly tumbles on a generalised planar Jeffery orbit depends only on W_{rot} , which can in turn depend strongly on the level of swimmer symmetry and the background flow. Hence, determining the angular dynamics of a swimmer involves detailed knowledge of both the swimmer and the background flow. In contrast, the character of the translational motion depends only on the flow and not on the properties

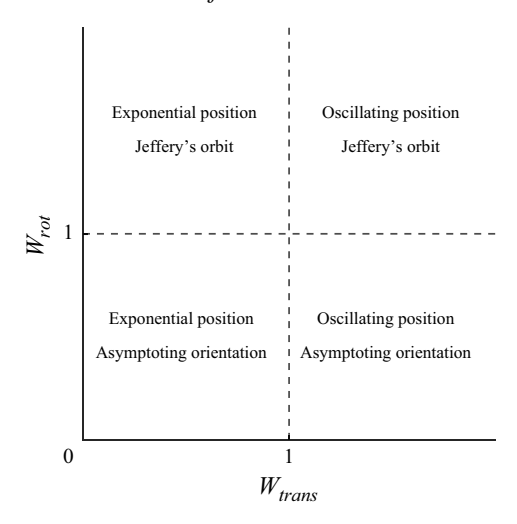


Figure 5. Long-time swimmer behaviours are a function of two effective parameters, defined in (7.1). One parameter, W_{trans} , depends only on the properties of the background flow and governs the translational dynamics; the other, W_{rot} , determines the orientational dynamics and depends on both the swimmer and the flow. Stationary shear flows fall on the line $W_{trans} = 1$, whilst flows that are irrotational on average (such as pure strain) correspond to $W_{rot} = 0$. This diagram neglects mathematically precise edge cases, which are considered thoroughly in §§ 4 and 5. Important special cases of resonance for W_{trans} and $W_{rot} > 1$ and the dynamics for the $W_{trans} = 1$ are also considered in table 3.

of the swimmer, splitting into trajectories that are exponential, oscillatory or linear in time based on the value of W_{trans} . In combination, these observations of angular dynamics and motility can extensively inform qualitative features of the swimmer trajectory. This ability to extensively classify the behaviours of a swimmer via only a two-dimensional (2-D) parameter space is much simpler than one might initially anticipate. A detailed summary of these behaviours, including some subcases, is presented in table 3, with examples of translational dynamics in each case shown in figure 6. We highlight that knowledge of the time-dependent shape parameters and self-induced velocities is key to applying the results of this study. To the best of our knowledge, these functions are unknown (but can in principle be calculated) for all but one microswimmer (*Chlamydomonas reinhardtii* (Omori *et al.* 2022)). Hence, in order to apply this understanding of swimmers in flows, a broad, classifying study of microswimmer shape and swimming profiles is warranted.

One can also immediately note instances where the interaction of the swimmer with the background flow can induce progressive motion even for reciprocal swimming, where no net motion is generated in the absence of background flow. This occurs with motion across pathlines for the linear, zero-mean oscillatory flows and shear flows of § 5.2 if the swimmer acquires a fixed angle at long time, as further illustrated for the special cases with an oscillating shear flow. Thus, the interaction of the swimmer with a background flow provides another means to break Purcell's scallop theorem that supplements other mechanisms, such as the introduction of viscoelasticity or inertia (Lauga 2007, 2011; Qiu, Lee & Mark 2014; Derr *et al.* 2022). Conversely, the characterisation of the swimmer also highlights when progressive swimming can be converted to oscillatory trajectories by the background flow, in particular for the linear zero-mean oscillatory flows of § 5.2, where the swimmer tumbles

As well as these general considerations, special cases of the dynamics for these swimmers in planar flows were considered, restricting attention to specific background

Angular dynamics	Translational dynamics	Trajectories and observations
Asymptoting or tumbling	Exponential $W_{trans} < 1$	The trajectory drifts to infinity at an exponential rate in the slow time scale once the average background flow strain rate dominates the average angular velocity, independent of the swimmer details. See figure $6(a)$.
Asymptoting $W_{rot} \leq 1$	Oscillating $W_{trans} > 1$	The long-time swimmer trajectory is an oscillation on the slow time scale of period $2\pi/(\overline{\Omega^*}^2 - \overline{E_{11}^*}^2 - \overline{E_{12}^*}^2)^{1/2}$. Progressive swimmer motion is converted to oscillatory motion by the background flow, independent of the swimmer details. See figure $6(b)$.
Tumbling $W_{rot} > 1$	Oscillating $W_{trans} > 1$	Whether the long-time dynamics is oscillatory or unbounded depends on whether resonance occurs. Resonance can require parameter fine-tuning, but not always, e.g. a body of revolution with fore—aft symmetry in a rotational background flow. See figure $6(c)$.
Asymptoting $W_{rot} \leq 1$	Linear, $\mathbf{A} = 0$, $W_{trans} = 1$	Trivial background flow is excluded. The swimmer will drift to infinity linearly in time if the net swimming speed V is non-zero. Infinite drift can also occur even if there is only reciprocal swimming, highlighting that Purcell's theorem can be broken by a zero-mean oscillatory flow. See figure $6(d)$.
Tumbling $W_{rot} > 1$	Linear, $\mathbf{A} = 0$, $W_{trans} = 1$	The swimmer does not drift to infinity, independent of the swimmer details, except fore—aft asymmetry is necessary to satisfy the tumbling condition. See figure $6(e)$.
Asymptoting $W_{rot} \leq 1$	Linear, $\mathbf{A} \neq 0$, $\mathbf{A}^2 = 0$, $W_{trans} = 1$	These flows are equivalent to a shear flow. The swimmer will drift to infinity, with even reciprocal swimming capable of generating motion perpendicular to the pathlines, breaking Purcell's theorem. See figure $6(f)$.
Tumbling $W_{rot} > 1$	Linear, $\mathbf{A} \neq 0$, $\mathbf{A}^2 = 0$, $W_{trans} = 1$	These flows are equivalent to a shear flow. The swimmer will drift to infinity along the pathlines but will not drift indefinitely perpendicular to the pathlines, independent of the swimmer details. See figure $6(g)$.

Table 3. A summary of swimmer behaviours in planar linear background flows. Edge cases, where parameter fine tuning leads to behaviours distinct from the more general cases, are not summarised here. Examples of corresponding swimming trajectories are shown in figure 6.

flows and highly symmetrical swimmers. Our first example considered a rotational flow, where tumbling is observed for the symmetric swimmer considered. In turn, this induced resonance once the swimmer had a non-zero net swimming speed $(V \neq 0)$. This also demonstrates that swimmer motility need not be converted to oscillations for sufficiently symmetric swimmers in rotating flows. Nonetheless, it is possible for the swimmer to enter the regime of an asymptoting angle despite the presence of a rotational background flow. For example, it may break fore–aft symmetry to rotate in the opposite direction to the background flow angular velocity. Then, in this regime, progressive motility is converted to oscillation (e.g. table 3). Hence, we can observe that, despite numerous observations in table 3 being independent of the details of the swimmer, aspects of inertialess motility in background flows can be sensitive to the details of the swimming gait. For instance, the gait may allow passage between the different types of behaviour in parameter space associated with the parameter groupings of (7.1).

For irrotational flows with a highly symmetric swimmer, we observe that the swimmer has an asymptoting angle for large time and the long-time trajectory forms a hyperbola

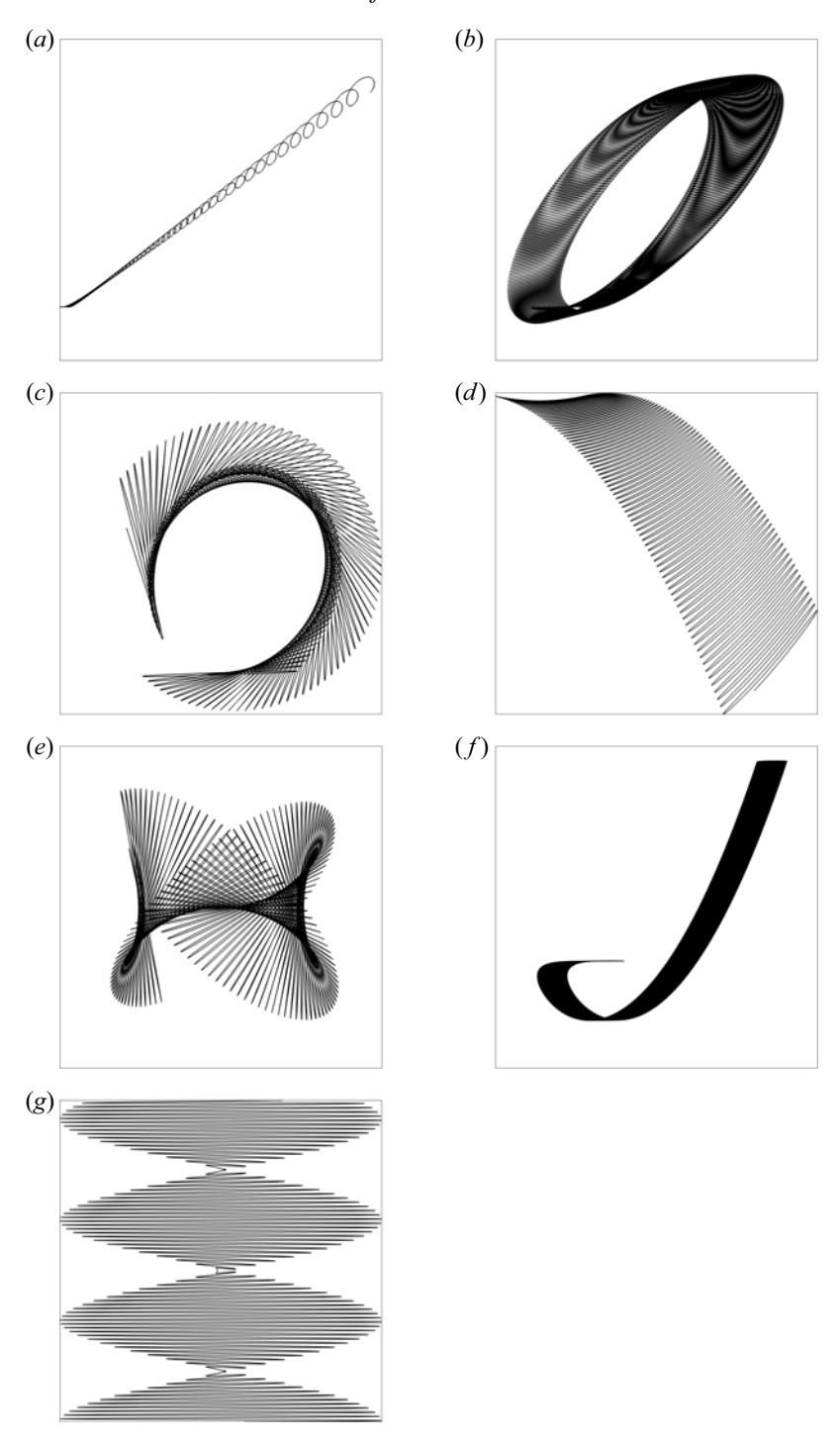


Figure 6. Example trajectories in the flow plane corresponding to the cases described in table 3, illustrating the variety of possible translational behaviours. Rapid oscillations and emergent long-time behaviours can be seen in all panels. Panels (a)—(g) correspond to rows 1–7 of table 3. Axes are scaled independently for visual clarity and all cases shown are reciprocal swimmers (V=0) with $\omega=50$. In (g), the observed net motion is along vertical flow pathlines.

in the plane of the flow. Furthermore, the observation of hyperbolic trajectories is robust to many features of the swimmer, though this can be disrupted by the introduction of a sufficiently large average angular velocity, $\Omega(T)$, induced by the swimmer in the absence of a background flow, which requires a fore–aft symmetry breaking of the swimmer.

In shear flows, there is in general a drift in the direction of fluid flow, but motility across pathlines is also possible. For stationary shear and a highly symmetric swimmer, this can only occur with extensive swimmer elongation, as such dynamics requires that the Bretherton parameter B satisfies $\overline{B}^2 > 1$. Otherwise, the dynamics across pathlines is oscillatory. In contrast, for background shear flows that have an oscillating contribution, such extreme elongation need not be required for indefinite drift across pathlines. More generally, for highly symmetric swimmers that do not tumble, the long-time trajectory is in the shape of a parabola, except for edge cases. Furthermore, if the mean shear flow is zero for a highly symmetric non-tumbling swimmer, the trajectory reduces to a line with unit gradient (given one axis is aligned along the direction of the flow and the convention of figure 1). The latter is one of many examples of the previously known observation that *a priori* averaging, that is the averaging of oscillations without considering the details of the particular model, can generate incorrect results, as reported for example by Walker *et al.* (2021, 2023).

While swimmers in shear flow have been subject to extensive study, for instance by Karp-Boss, Boss & Jumars (2000), Hope *et al.* (2016*b*), Gaffney *et al.* (2022*a*) and Walker *et al.* (2022*a*), we see that swimmer behaviour in a pure steady shear flow truly is a special case. The introduction of oscillations can fundamentally change the character of swimmer behaviour, leading to parabolic trajectories emerging. Similarly, small changes to the background flow can extensively change the swimmer behaviour. For example, a small change in the flow so that the flow angular velocity dominates the rate of strain (if only weakly) induces an oscillatory motion of a non-tumbling swimmer rather than a drifting motion. In contrast, if the small change is such that the rate of strain dominates then there is a drift to infinity, as may be inferred from the summaries of figure 5 or table 3.

This raises the question of how further changes in the flow influence swimmer dynamics. A pertinent question concerns rheotaxis, which has been observed and predicted for swimmers in a Poiseuille flow (Omori et al. 2022; Walker et al. 2022b) and sperm cells under relatively general circumstances, for instance swimming in shear flows (Miki & Clapham 2013; Kantsler et al. 2014; Ishimoto & Gaffney 2015), as well as predicted for squirmers close to a no-slip wall (Uspal et al. 2015; Ishimoto 2017). These observations, however, do not fall into the remit of the analysis presented here in that they involve a reorientation in the swimming plane, perpendicular to $e_3 = \hat{e}_3$, due to a flow that varies in the e_3 direction, while we have only considered flows that are in the swimming plane and not perpendicular to it, except for the trivial case of a constant flow in this direction. Hence, such observations do not contradict the observation here that, at leading order in $1/\omega$, no predictions of rheotaxis have emerged for a swimmer in a plane in response to a linear flow restricted to the same plane. The absence of rheotaxis is illustrated by the hyperbola and the parabola of (6.10) and (6.18) in special cases, for example, and is also apparent from the prediction that the final swimming direction angle for an asymptoting swimmer depends on the initial swimming direction, as may be inferred from (3.16). The consideration of nonlinear flows, surfaces and spatially non-constant flow angular velocities and rates of strain are further pertinent examples left for future work. In particular, such features may induce behaviours profoundly different from those observed here, with one example concerning angular rocking back and forth, which is not present in the scope of the dynamics considered here, but nonetheless has been observed in the oscillating rheotaxis

of artificial swimmers in response to Poiseuille flows within small microchannels (Dey et al. 2022).

Since individual dynamics often feature in the construction of population models for swimmers (Ezhilan et al. 2013; Saintillan & Shelley 2013; Junot et al. 2019), this study also offers the prospect of facilitating the development of collective swimmer models in more general background flows than has typically been considered. Furthermore, given the classification of swimmer behaviours, one can also consider how one may control a swimmer (or mobile microrobot) in a background flow, assuming that it cannot swim with sufficient speed to render the background flow as a small perturbation that can be ignored in terms of navigation. In particular, manipulating the swimmer cannot control the trichotomy of the translational dynamics (into those of exponential, oscillating and linear character) as these depend only on the background flow. However, the swimmer can always, at least in principle, be switched from tumbling to asymptoting in its angular behaviour, for instance by controlling its self-induced rotation $\Omega(T)$. While such switching does not have an impact on the exponential translation case, switching to tumbling angular dynamics in the case of linear translation increases the prospect of localised trajectories rather than drifting, with potentially the opposite for oscillating flows if a resonance occurs in the latter case with tumbling, as again may be inferred from table 3.

A final direction concerns the extent to which this study generalises on relaxing the swimmer symmetry restrictions of § 2.3, which are further documented in Appendix B. This is an open question. Further progress may possibly be feasible using a generic approach, such as that of Gaffney *et al.* (2022*b*). However, some restriction is likely to be required for progress, as the more general case couples in-plane and out-of-plane dynamics. One less-symmetric instance where it might nonetheless be possible to make further progress concerns swimmers whose shapes throughout the gait cycle have only two planes of symmetry, as studied by Thorp & Lister (2019). However, assessing the extent to which, and how, the results presented here may extend to less symmetric swimmers requires detailed investigation and is beyond the scope of the present study. Similarly, an investigation of the role of stochastic effects would also be pertinent, especially given the observed effects of noise on passive Jeffery orbits (Talbot *et al.* 2024).

In summary, the equations of motion for a swimmer possessing modest spatial symmetry in a linear planar background flow have been derived using the assumption of inefficiency. That is, we have assumed that the swimmer's net motion is much slower than the deformations and treadmilling required to generate its motion, noting that this is commonplace in microswimming. The resulting solutions allow for a classification of swimmer behaviour based on just two key parameters, W_{rot} and W_{trans} of (7.1), which measure the ratio of the background flow angular velocity to rate of strain, and the ratio of the swimmer and flow angular velocity to the swimmer's interaction with the flow rate of strain. Thus, via this multiscale analysis, we have demonstrated that this complex system can be extensively understood in terms of only two degrees of freedom. Furthermore, the present study highlights the need both for detailed measurement of time-dependent swimmer properties and careful averaging in analysing the equations of motion, whilst observing that the interactions between a swimmer and a background flow can provide a further mechanism for circumventing Purcell's scallop theorem. Common, nearly universal behaviours are also predicted, such as long-time parabolic trajectories for swimmers in oscillatory shear flows. Furthermore, the examples considered here highlight when swimmer navigation in background flows is futile, together with when and how the swimmer is capable of switching from localised trajectories to inexorable drift, or vice versa, enabling an element of rational control over swimmer and microrobot movement in linear background flows.

Funding. K.I. acknowledges the Japan Society for the Promotion of Science (JSPS) KAKENHI (grant no. 21H05309) and the Japan Science and Technology Agency (JST), FOREST (grant no. JPMJFR212N). B.J.W. is supported by the Royal Commission for the Exhibition of 1851.

Declaration of interests. The authors report no conflict of interest.

Data availability statement. All codes used to generate figures in this manuscript are available at https://github.com/Mar5bar/multi-timescale-microswimmers-in-background-flows. For the purpose of Open Access, the authors will apply a CC BY public copyright licence to any Author Accepted Manuscript (AAM) version arising from this submission.

Appendix A. Deriving the governing equations

Here, we derive the governing equations for the translation and rotation of shape changing and treadmilling swimmers in time-dependent planar linear background flows, assuming that the swimmer moves in the plane of the flow and with sufficient swimmer symmetry, as detailed in $\S 2.3$, to ensure a relatively simple generalisation of idealised models. We first reduce the problem to that of treating the swimmer at a fixed time as a rigid particle, enabling rigid particle methods, such as that presented in the appendices of Dalwadi *et al.* (2024*b*).

We inherit the notation of the main text, for example with $\mathbf{x} = x\mathbf{e}_1 + y\mathbf{e}_2 + z\mathbf{e}_3$ denoting the position of a point relative to the laboratory-frame basis, $\{\mathbf{e}_1, \mathbf{e}_2, \mathbf{e}_3\}$, while $\{\hat{\mathbf{e}}_1, \hat{\mathbf{e}}_2, \hat{\mathbf{e}}_3\}$ denotes the swimmer frame basis, with origin at \mathbf{x}_c , the swimmer centroid. Hence,

$$\hat{\boldsymbol{e}}_1 = \cos\theta \boldsymbol{e}_1 + \sin\theta \boldsymbol{e}_2, \quad \hat{\boldsymbol{e}}_2 = -\sin\theta \boldsymbol{e}_1 + \cos\theta \boldsymbol{e}_2, \quad \hat{\boldsymbol{e}}_3 = \boldsymbol{e}_3, \tag{A1}$$

and the background flow field is given by

$$\boldsymbol{u}^*(\boldsymbol{x},T) = \boldsymbol{u}_{tr}^*(T) + \boldsymbol{\Omega}^*(T) \wedge \boldsymbol{x} + \boldsymbol{E}^*(T)\boldsymbol{x}$$
(A2a)

$$= \boldsymbol{u}_c^* + \boldsymbol{\Omega}^*(T) \wedge (\boldsymbol{x} - \boldsymbol{x}_c) + \boldsymbol{E}^*(T)(\boldsymbol{x} - \boldsymbol{x}_c), \tag{A2b}$$

where $T = \omega t$ is the fast time scale, $\boldsymbol{u}_{tr}^*(T)$ denotes the spatially constant translational aspect of the background flow. Here, $\boldsymbol{E}^*(T)$ and $\boldsymbol{\Omega}^*(T)$ denote the rate of strain and angular velocity, respectively, which are spatially constant by flow linearity. Below, we use $\boldsymbol{u}_c^* = \boldsymbol{u}^*(\boldsymbol{x}_c(t,T),T)$ to denote the background flow at the swimmer centroid if the swimmer was absent from the domain.

A.1. Model mechanics and the grand mobility tensor

With u denoting the velocity vector field of the flow including the swimmer, in contrast to the background flow u^* which excludes the swimmer, we have that the fundamental equations for the displacement flow, $u^{d_p} = u - u^*$, with disturbance pressure p^{d_p} are given by

$$\nabla p^{d_p} = \nabla^2 \boldsymbol{u}^{d_p}, \quad \nabla \cdot \boldsymbol{u}^{d_p} = 0, \tag{A3}$$

exterior to the particle with decay boundary conditions at spatial infinity. Noting that the swimmer shape deformations and treadmilling are independent of the external flow, the boundary conditions for u on the swimmer surface, $x \in \partial \Lambda$, are given by

$$u^{d_{p}}(x) = u^{S}(x, T) + U(T, u^{*}) + \Omega(T, u^{*}) \wedge (x - x_{c}) - u^{*}(x, T),$$

$$= u^{S}(x, T) + \left[U(T, u^{*}) - u_{c}^{*}\right]$$

$$+ \left[\Omega(T, u^{*}) - \Omega^{*}(T)\right] \wedge (x - x_{c}) - E^{*}(T)(x - x_{c}).$$
(A4a)

Here, $x_c = x_c(t, T)$ is the location of the swimmer centroid and $u_c^* = u_c^*(x_c(t, T), T)$ is the background flow at the swimmer centroid. In addition, $u^S(x, T)$ is the surface

velocity, accommodating shape-shifting and tread-milling, which is 2π -periodic in T, while $U(T, u^*)$ denotes the swimming speed of the particle in the background flow, u^* , at time T. Also, $\Omega(T, u^*)$ denotes the angular velocity of the body fixed frame relative to the inertial frame in the background flow, $u^*(x, T)$.

As the linear velocity and angular velocity are six degrees of freedom in the unknowns, six further constraints are required; assuming the swimmer is not also being driven by an external forcing, such as a magnetic field, these are no net force and torque, that is

$$\int_{\partial A} \boldsymbol{\sigma} \cdot \boldsymbol{n} \, dS = \int_{\partial A} (\boldsymbol{x} - \boldsymbol{x}_c) \wedge \boldsymbol{\sigma} \cdot \boldsymbol{n} \, dS = \boldsymbol{0}, \tag{A5}$$

where n is the normal, defined to point out of the fluid domain, and

$$\boldsymbol{\sigma} = -p^{d_p} \boldsymbol{I} + (\nabla \boldsymbol{u}^{d_p} + (\nabla \boldsymbol{u}^{d_p})^{\top}) \tag{A6}$$

is the Cauchy stress. A pressure gauge condition is also required to pin the translational freedom in the pressure $p^{d_p} \mapsto p^{d_p} + \text{constant}$.

We decompose the disturbance problem, (A3) to (A5), into two auxiliary problems for the pressure and velocity fields $(p^{d_1}, \boldsymbol{u}^{d_1})$ and $(p^{d_2}, \boldsymbol{u}^{d_2})$, respectively. The first auxiliary problem is for the swimmer shape at fixed time T, with the shape pinned within quiescent fluid without the freedom to translate or rotate, but nonetheless undergoing the shape shifting and treadmilling surface changes. Thus, the bulk equations, (A3), are inherited as are the decay boundary conditions at spatial infinity, but the velocity boundary condition becomes

$$\boldsymbol{u}^{d_1} = \boldsymbol{u}^S(\boldsymbol{x}, T), \quad \boldsymbol{x} \in \partial \Lambda. \tag{A7}$$

Given a pressure gauge fixing, no further force or torque constraints are required, as the constraints are now the absence of translation and rotation. Let F(T) define the force required to be imposed on the particle (for example by microtweezers in practice) to enforce these constraints, and analogously for T(T). The net force and torque on the particle must be zero in the inertialess limit and, hence,

$$\int_{\partial A} \boldsymbol{\sigma}^{d_1} \cdot \boldsymbol{n} \, dS + \boldsymbol{F}(T) = \boldsymbol{0}, \quad \int_{\partial \int_{\partial A}} (\boldsymbol{x} - \boldsymbol{x}_c) \wedge \boldsymbol{\sigma}^{d_1} \cdot \boldsymbol{n} \, dS + \boldsymbol{T}(T) = \boldsymbol{0}.$$
 (A8)

The second auxiliary problem similarly inherits the bulk Stokes equations, (A3), the decay boundary conditions at spatial infinity and the pressure gauge condition. However, with fixed t, T, the velocity boundary condition is taken to be

$$\boldsymbol{u}^{d_2}(\boldsymbol{x}) = \left[\boldsymbol{U}(T, \boldsymbol{u}^*) - \boldsymbol{u}_c^*\right] + \left[\boldsymbol{\Omega}(T, \boldsymbol{u}^*) - \boldsymbol{\Omega}^*(T)\right] \wedge (\boldsymbol{x} - \boldsymbol{x}_c) - \boldsymbol{E}^*(T)(\boldsymbol{x} - \boldsymbol{x}_c), \tag{A9}$$

where $U(T, u^*)$ is the *a priori* unknown translation speed of the particle in the background flow at this instant for this problem, and $\Omega(T, u^*)$ is the *a priori* unknown angular velocity of the swimmer frame relative to the inertial frame in the background flow for this problem. The six additional constraints are taken to be

$$\int_{\partial A} \boldsymbol{\sigma}^{d_2} \cdot \boldsymbol{n} \, dS = \boldsymbol{F}(T), \quad \int_{\partial A} (\boldsymbol{x} - \boldsymbol{x}_c) \wedge \boldsymbol{\sigma}^{d_2} \cdot \boldsymbol{n} \, dS = \boldsymbol{T}(t), \quad (A10)$$

so that $(p^{d_1} + p^{d_2}, \mathbf{u}^{d_1} + \mathbf{u}^{d_2})$ provide a solution of the original problem, which is unique given pressure gauge fixing and, thus, this is the solution. Hence, $U(T, \mathbf{u}^*)$ and $\Omega(T, \mathbf{u}^*)$ in the solution of the above second auxiliary problem are also the swimming speed and angular velocity of the shape shifting and tread-milling swimmer in the background flow.

Note that, in the second auxiliary problem, the velocity boundary condition is that of a rigid particle, with an unknown net force and an unknown net torque prescribed, which can be framed in the setting of the 'grand mobility tensor' framework of Kim & Karrila (2005). In particular, we proceed by first considering the behaviour of the swimmer in a quiescent fluid, before then investigating the swimmer dynamics in the background flow, under the assumption that the shape-shifting and tread-milling are unchanged in the presence or absence of the background flow.

In the absence of a background flow, $u_c^* = \Omega^* = 0$, $E^* = 0$ and the surface velocity $u^S(T)$ induce a swimming speed U(T, 0) and angular velocity $\Omega(T, 0)$. In the framework of the grand mobility tensor of Kim & Karrila (2005) for the second auxiliary problem, with a trivial background flow, we have at time T that

$$\begin{bmatrix} -U(T, \mathbf{0}) \\ -\Omega(T, \mathbf{0}) \\ S \end{bmatrix} = \begin{bmatrix} \mathbf{A}(T) & \tilde{\mathbf{b}}(T) & \tilde{\mathbf{g}}(T) \\ \mathbf{b}(T) & \mathbf{c}(T) & \tilde{\mathbf{h}}(T) \\ \mathbf{g}(T) & \mathbf{h}(T) & \mathbf{m}(T) \end{bmatrix} \begin{bmatrix} F(T) \\ T(T) \\ \mathbf{0} \end{bmatrix}, \tag{A11}$$

where the T-dependent block entries of the grand mobility tensor relate the force, F(T), to the velocity of the particle in a quiescent field. While not used here, S denotes the stresslet associated with the particle motion. Reinstating the background flow with the shape shifting and treadmilling assumed unchanged, so that F(T), T(T) and the grand mobility tensor associated with the second auxiliary problem are invariant with the change of external flow, the analogous Kim & Karrila (2005) relation with a background flow is given by

$$\begin{pmatrix}
\mathbf{u}_{c}^{*} - \mathbf{U}(T, \mathbf{u}^{*}) \\
\mathbf{\Omega}^{*} - \mathbf{\Omega}(T, \mathbf{u}^{*}) \\
\mathbf{S}^{*}
\end{pmatrix} = \begin{bmatrix}
\mathbf{A}(T) & \tilde{\mathbf{b}}(T) & \tilde{\mathbf{g}}(T) \\
\mathbf{b}(T) & \mathbf{c}(T) & \tilde{\mathbf{h}}(T) \\
\mathbf{g}(T) & \mathbf{h}(T) & \mathbf{m}(T)
\end{bmatrix} \begin{bmatrix}
\mathbf{F}(T) \\
T(T) \\
\mathbf{E}^{*}
\end{bmatrix},$$
(A12)

where S^* denotes the stresslet associated with the particle motion in the planar, background flow.

A.2. The swimmer velocity and the governing equations

The objective is to use (A11) and (A12) to determine $U(T, u^*)$ and $\Omega(T, u^*)$, thus yielding the equation of motion. This requires us to specify $U(T, \mathbf{0})$, the linear velocity of the swimmer in the absence of flow, and $\Omega(T, \mathbf{0})$, the angular velocity of the swimmer in the absence of flow. The linear velocity scales with the frequency of the shape deformations and treadmilling by the linearity of Stokes flow and the fact that time is simply a parameter in the absence of temporal derivatives. Thus, we can write the velocity of the swimmer for $u^* = 0$ in the form

$$U(T,0) = \omega U(T)\hat{\mathbf{e}}_1 + \omega V^* \hat{\mathbf{e}}_1, \tag{A13}$$

where $\omega \gg 1$ is the scale of the swimmer deformation speed relative to the background flow speed, ωV^* is the average speed along the body axis and U(T) is the swimmer oscillatory speed, along its swimming direction, \hat{e}_1 . The latter averages to zero over a period, taken to be 2π without loss of generality.

While $\omega |V^*| \sim \omega \sup_T |U(T)|$ has been considered in previous analytically based multiple time scale studies of swimmers in background flow (Walker *et al.* 2022*b*), many swimmers are inefficient and have small net swimming speeds compared with the velocity of oscillatory motions, or even a zero net-swimming speed in the case of reciprocal swimmers. This separation of scales is observed for many theoretical swimmers

(Curtis & Gaffney 2013; Ishimoto & Gaffney 2014; Pak & Lauga 2015), with the three-link swimmer an extreme example (Curtis & Gaffney 2013), while it also observed for biological microswimmers. For example, considering the experimental observations of sperm in Smith *et al.* (2009), and restricting attention to the effectively Newtonian, low-viscosity medium, the progressive velocity of the cell is $62\mu m s^{-1}$, while its flagellar wavespeed is $920\mu m s^{-1}$.

Hence, we consider scales where

$$\omega |V^*| \ll \omega \sup_{T} |U(T)|.$$
 (A14)

For many cases, $\omega |V^*| \ll 1$ is not of interest, as the swimmer will be washed out by the background flow, noting the latter has an ord(1) velocity scale by the non-dimensionalisation. However, analysing whether Purcell's scallop theorem generalises to include swimmer-flow interactions specifically concerns reciprocal swimmers with $V^*=0$, so this case is also investigated in the main text. We also impose the restriction that $\omega |V^*| \gg 1$, so that there is a substantive interaction between the swimmer and the flow, rather than the swimmer being only weakly perturbed by the flow. Hence, we have

$$U(T,0) = \omega U(T)\hat{\boldsymbol{e}}_1 + V\hat{\boldsymbol{e}}_1, \quad |V| \sim O\left(\sup_T |U(T)|\right) \sim O(1). \quad (A15)$$

We additionally note that any corrections at higher powers of $1/\omega \ll 1$ will not feature in the equations once the multiple scales approximation has been taken. Then, with use of (A11) to eliminate F(T) and T(T), we have from (A12) that the governing equations for the particle velocity and angular velocity in the shear flow are given by

$$\frac{\mathrm{d}\boldsymbol{x}_c}{\mathrm{d}t} = \boldsymbol{U}(T, \boldsymbol{u}^*) = \boldsymbol{u}_c^* + \omega U(T)\hat{\boldsymbol{e}}_1 + V\hat{\boldsymbol{e}}_1 - \tilde{\boldsymbol{g}}\boldsymbol{E}^*. \tag{A16}$$

Considering the angular dynamics, the restriction to planar dynamics ensures that we can write

$$\mathbf{\Omega}(T, \mathbf{u}^*) = \dot{\theta} \mathbf{e}_3 = \dot{\theta} \hat{\mathbf{e}}_3, \quad \mathbf{\Omega}^*(T) = \mathbf{\Omega}^*(T) \hat{\mathbf{e}}_3, \quad \mathbf{\Omega}(T, \mathbf{0}) = \mathbf{\Omega}(T, \mathbf{0}) \hat{\mathbf{e}}_3.$$
 (A17)

The term $\Omega(T, \mathbf{0})$ represents the angular velocity induced by the shape deformation when the swimmer is not in a background flow. As these deformations may be on the fast time scale, we can write

$$\Omega(T, \mathbf{0}) = \omega \Omega_f(T) + \Omega(T), \tag{A18}$$

where $\Omega_f(T)$ is the zero-mean angular velocity on the fast time scale and $\Omega(T)$ is the first correction in the expansion of $\Omega(T, \mathbf{0})$ in powers of $1/\omega \ll 1$. In particular, we maintain generality by including the possibility of a contribution at ord(1), analogously to the inefficient contribution to translation motion. Similarly, contributions at higher orders of $1/\omega \ll 1$ do not contribute once the multiple scales approximation has been imposed.

Noting the memoryless property of Stokes flow, both $\Omega_f(T)$, $\Omega(T)$ inherit the periodicity of the shape deformation and, thus, are both 2π -periodic. Then, eliminating F(T) and T(T) analogously to the derivation of (A16), we have

$$\dot{\theta} \boldsymbol{e}_3 = \dot{\theta} \hat{\boldsymbol{e}}_3 = \boldsymbol{\Omega}(T, \boldsymbol{u}^*) = \boldsymbol{\Omega}^*(T) + \boldsymbol{\Omega}(T, \boldsymbol{0}) - \tilde{\boldsymbol{h}} \boldsymbol{E}^*$$
(A19a)

$$= \Omega^*(T)\hat{\boldsymbol{e}}_3 + [\omega\Omega_f(T) + \Omega(T)]\hat{\boldsymbol{e}}_3 - \tilde{\boldsymbol{h}}\boldsymbol{E}^*. \tag{A19b}$$

Noting the assumption of planarity used in the above, we also require $\hat{h}E^*$ to be parallel to $\hat{e}_3 = e_3$. While not assured for general particle shapes, this is guaranteed by only relatively weak symmetry constraints on the swimmer (which must apply throughout its entire

deformation), such as those detailed in § 2.3 and Appendix B. Finally, while rotation out of the plane of flow is not admissible, translation perpendicular to the plane of flow (with the symmetry broken by the swimmer shape) can be accommodated, so that we do not a priori require that $-\tilde{\mathbf{g}}\mathbf{E}^*$ has no component perpendicular to the flow plane. In § 2.3, we simplify $-\tilde{\mathbf{h}}\mathbf{E}^*$ and $-\tilde{\mathbf{g}}\mathbf{E}^*$ and proceed to explore the resulting equations of motion. Finally, in the main text around (3.23), we note that inefficiency forces a further constraint, in particular that the combination of fast rotational oscillations and fast (but zero-average) translational dynamics do not interact to produce a net fast swimming speed.

Appendix B. Admissible swimmer shapes

Here, we describe various classes of swimmer shapes that are admissible within the framework of this manuscript.

B.1. The
$$C_{nv}$$
 bodies

These are swimmer shapes that, for all times of the gait cycle, possess a helicoidal symmetry of degree $n \ge 3$ along with n reflection planes containing the helicoidal axis. For such bodies, we have

$$\eta_2 = 0, \quad \lambda_2 \equiv -B, \quad \lambda_5, \ \eta_3, \ \eta_4 \neq 0$$
(B1)

for n = 3, while for $n \ge 4$ we have

$$\lambda_5 = \eta_2 = 0, \quad \lambda_2 \equiv -B, \quad \eta_3, \ \eta_4 \neq 0.$$
 (B2)

B.2. The
$$C_{nh}$$
 bodies

These swimmers are a subset of C_{nv} bodies and possess an additional reflection symmetry perpendicular to the helicoidal axis, i.e. a fore–aft symmetry. With this, we have

$$\Omega_f(T) = \Omega(T) = \lambda_5 = \eta_2 = \eta_3 = 0, \quad \lambda_2 \equiv -B, \quad \eta_4 \neq 0$$
 (B3)

for n = 3, while for $n \ge 4$ we have

$$\Omega_f(T) = \Omega(T) = \lambda_5 = \eta_2 = \eta_3 = \eta_4 = 0, \quad \lambda_2 \equiv -B \neq 0.$$
 (B4)

Note that the fore–aft symmetry of such swimmers also entails that the angular velocity in the absence of flow must be zero, as this would otherwise break fore–aft symmetry. Hence, we also have $\Omega_f(T) = \Omega(T) = 0$ for these swimmers.

B.3. The
$$D_n$$
 bodies

This class of bodies includes swimmer shapes that, for all times of the gait cycle, possess a helicoidal symmetry of degree $n \ge 4$. In addition, they possess dihedral symmetry associated with n-axes perpendicular to the helicoidal axis, around which a rotation of π leaves the body invariant. Then, we have

$$\lambda_5 = \eta_3 = 0, \quad \lambda_2 \equiv -B, \quad \eta_2, \, \eta_4 \neq 0.$$
 (B5)

B.4. The
$$D_{nh}$$
 bodies

These swimmers are a subset of D_n bodies and additionally possess a reflection symmetry perpendicular to the helicoidal axis, that is a fore–aft symmetry. Then we have

$$\Omega_f(T) = \Omega(T) = \lambda_5 = \eta_2 = \eta_3 = 0, \quad \lambda_2 \equiv -B, \, \eta_4 \neq 0.$$
 (B6)

B.5. Bodies of revolution

Swimmers that are bodies of revolution satisfy the symmetries of both the D_n and C_{nv} $(n \ge 4)$ bodies and, when possessing additional fore–aft symmetry, the symmetries of both the D_{nh} and C_{nh} $(n \ge 4)$ bodies. In general, however, there are no further simplifications.

Thus, we have the translational equation of motion

$$\frac{\mathrm{d}\boldsymbol{x}_{c}}{\mathrm{d}t} = \boldsymbol{u}_{c}^{*} + \omega U(T)\hat{\boldsymbol{e}}_{1} + V\hat{\boldsymbol{e}}_{1} - \eta_{2}(T)\hat{E}_{12}^{*}(T, \sin 2\theta, \cos 2\theta)\hat{\boldsymbol{e}}_{3}
+ \eta_{3}(T)\boldsymbol{B}_{0}(T, \sin 2\theta, \cos 2\theta)\hat{\boldsymbol{e}}_{1} - \eta_{4}(T)\hat{E}_{22}^{*}(T, \sin 2\theta, \cos 2\theta)\hat{\boldsymbol{e}}_{2},$$
(B7)

with

$$\boldsymbol{B}_{0}(T, \sin 2\theta, \cos 2\theta) = \boldsymbol{E}^{*}(T) - [E_{11}^{*}(T)\cos 2\theta + E_{12}^{*}(T)\sin 2\theta] \left(\boldsymbol{e}_{1}\boldsymbol{e}_{1}^{\top} + \boldsymbol{e}_{2}\boldsymbol{e}_{2}^{\top}\right)$$
(B8)

in this case. Analogously, the angular equation of motion simplifies to

$$\frac{d\theta}{dt} = \Omega^*(T) + \omega \Omega_f(T) + \Omega(T) + [\lambda_5(T) E_{12}^*(T) - B(T) E_{11}^*(T)] \sin 2\theta
+ [\lambda_5(T) E_{11}^*(T) + B(T) E_{12}^*(T)] \cos 2\theta.$$
(B9)

Appendix C. Symmetry simplifications of the leading-order multiscale equations of motion

Here, we consider further simplifications to the leading-order multiscale equations of motion given by (3.13) and (3.40) once the swimmer possesses additional symmetries or does not have a rapid oscillatory motion in a quiescent fluid.

C.1. Fore–aft symmetry and the absence of fast rotation

Suppose that there is no self-induced rapid oscillatory rotation ($\Omega_f = 0$), so that the swimmer rotation rate in a quiescent fluid reduces to

$$\Omega(T, \mathbf{0}) = \left[\omega \Omega_f(T) + \Omega(T)\right] e_3 = \Omega(T) e_3. \tag{C1}$$

Then, we have $\Psi = 0$ and, hence, for the angular equations we have

$$\theta_0(t,T) = \overline{\theta}_0(t) = \tilde{\theta}_0(t).$$
 (C2)

As a result, the leading-order angular dynamics is no longer displaced from the fast time scale average $\overline{\theta}_0(t)$, which reduces the complexity of the rotational and translational equations substantially.

Firstly, (3.10) reduces to

$$b_{\ddagger}(T) = B(T)E_{11}^{*}(T) - \lambda_{5}(T)E_{12}^{*}(T) = b_{\dagger}(T),$$
 (C3a)

$$c_{\ddagger}(T) = -B(T)E_{12}^{*}(T) - \lambda_{5}(T)E_{11}^{*}(T) = c_{\dagger}(T).$$
 (C3b)

Hence, the leading-order angular equation takes the same form as before, i.e.

$$\frac{d\overline{\theta}_0}{dt} = a - b\sin 2\overline{\theta}_0 - c\cos 2\overline{\theta}_0, \quad a = \overline{a}_{\dagger}, \ b = \overline{b}_{\ddagger}, \ c = \overline{c}_{\ddagger}, \tag{C4}$$

where the fast-time averages $b = \overline{b}_{\ddagger}$ and $c = \overline{c}_{\ddagger}$ that classify the rotational equations of motion are simplified significantly according to (C3). Nonetheless, the interpretation that they represent measures of the rate of strain of the background flow, modulated by swimmer properties, is still retained.

Considering the translational equation (3.36), we have the further simplifications that

$$U_s(T) = I_{Us}(T) = V_{Us} = 0, \quad U_c(T) = U(T), \quad V_{Uc} = \omega \overline{U \cos \Psi} = \omega \overline{U} = 0,$$

$$\chi(T) = a_{\dagger}(T) - b_{\dagger}(T) \sin 2\overline{\theta}_0 - c_{\dagger}(T) \cos 2\overline{\theta}_0$$
 (C5)

and, thus,

$$\hat{\boldsymbol{e}}_{10}(\overline{\theta}_0) = \cos \overline{\theta}_0 \boldsymbol{e}_1 + \sin \overline{\theta}_0 \boldsymbol{e}_2 = \tilde{\boldsymbol{e}}_{10}(\tilde{\theta}_0), \tag{C6}$$

$$\hat{\boldsymbol{e}}_{20}(\overline{\theta}_0) = -\sin\overline{\theta}_0\boldsymbol{e}_1 + \cos\overline{\theta}_0\boldsymbol{e}_2 = \tilde{\boldsymbol{e}}_{20}(\tilde{\theta}_0). \tag{C7}$$

Taking $\overline{u_{tr}^*} = 0$ without loss of generality by choice of the inertial reference frame, we have that (3.36) for the motion in the plane of the flow reduces to

$$\frac{d\overline{x}_{0}}{dt} = A\overline{x}_{0} + \left[\overline{I_{Uc}A} + VI + \overline{\eta_{3}(T)B_{0}(T, \sin 2\overline{\theta}_{0}, \cos 2\overline{\theta}_{0})}\right] \hat{e}_{10}(\overline{\theta}_{0})$$

$$- \left[\overline{\eta_{4}\hat{E}_{22}^{*}(T, \sin 2\overline{\theta}_{0}, \cos 2\overline{\theta}_{0})} + \overline{\chi}\overline{I_{Uc}}\right] \hat{e}_{20}(\overline{\theta}_{0})$$

$$= \left[\frac{\overline{E}_{11}^{*}}{\overline{E}_{12}^{*}} + \overline{\Omega^{*}} - \overline{E}_{11}^{*}\right] \overline{x}_{0} + V\hat{e}_{10}(\overline{\theta}_{0})$$

$$- \left[\overline{I_{Uc}\Omega} - \overline{I_{Uc}b_{\dagger}} \sin 2\overline{\theta}_{0} - \overline{I_{Uc}c_{\dagger}} \cos 2\overline{\theta}_{0}\right] \hat{e}_{20}(\overline{\theta}_{0})$$

$$+ \left[(\overline{\eta_{4}E_{11}^{*}} + \overline{\eta_{3}E_{12}^{*}}) \cos 2\overline{\theta}_{0} + (\overline{\eta_{4}E_{12}^{*}} - \overline{\eta_{3}E_{11}^{*}}) \sin 2\overline{\theta}_{0}\right] \hat{e}_{20}(\overline{\theta}_{0})$$

$$+ \left[\frac{\overline{I_{Uc}E_{11}^{*}}}{\overline{I_{Uc}E_{12}^{*}}} - \overline{\overline{I_{Uc}E_{12}^{*}}}\right] \hat{e}_{10}(\overline{\theta}_{0}).$$
(C9)

C.2. *The equations of motion for a body of revolution with fore–aft symmetry* For a body of revolution with fore–aft symmetry we additionally have

$$\lambda_5 = \Omega(T) = \eta_2 = \eta_3 = \eta_4 = 0,$$
 (C10)

so that the influence of the rate of strain is only through the Bretherton parameter $B(T) \equiv -\lambda_2(T)$. Then, with $\overline{u_{tr}^*} = \mathbf{0}$ by the choice of the inertial reference frame, the translational equations of motion further simplify to

$$\frac{\mathrm{d}\overline{z}_0}{\mathrm{d}t} = 0,\tag{C11}a$$

$$\frac{\mathrm{d}\overline{x}_0}{\mathrm{d}t} = \mathbf{A}\overline{x}_0 + \left[\overline{I_{Uc}\mathbf{\Lambda}} + V\mathbf{I}\right]\hat{\mathbf{e}}_{10}(\overline{\theta}_0) - \overline{\chi I_{Uc}}\hat{\mathbf{e}}_{20}(\overline{\theta}_0)$$
(C11b)

$$= \mathbf{A}\overline{x}_{0} + (\overline{I_{Uc}BE_{11}^{*}} \sin 2\overline{\theta}_{0} - \overline{I_{Uc}BE_{12}^{*}} \cos 2\overline{\theta}_{0})\hat{\mathbf{e}}_{20}(\overline{\theta}_{0})
+ \begin{bmatrix} V + \overline{I_{Uc}E_{11}^{*}} & \overline{I_{Uc}E_{12}^{*}} \\ \overline{I_{Uc}E_{12}^{*}} & V - \overline{I_{Uc}E_{11}^{*}} \end{bmatrix} \hat{\mathbf{e}}_{10}(\overline{\theta}_{0}).$$
(C11c)

REFERENCES

BACHELOR, G.K. 1967 An Introduction to Fluid Dynamics. CUP.

Bretherton, F.P. 1962 The motion of rigid particles in a shear flow at low Reynolds number. *J. Fluid Mech.* **14** (2), 284–304.

CHENGALA, A., HONDZO, M. & SHENG, J. 2013 Microalga propels along vorticity direction in a shear flow. Phys. Rev. E 87, 052704.

- CURTIS, M.P. & GAFFNEY, E.A. 2013 Three-sphere swimmer in a nonlinear viscoelastic medium. *Phys. Rev.* E 87, 043006.
- DALWADI, M.P. 2025 Rapidly yawing spheroids in viscous shear flow: emergent loss of symmetry. J. Fluid Mech. 1009, A27.
- DALWADI, M.P., ISHIMOTO, K., MOREAU, C., GAFFNEY, E.A. & WALKER, B.J. 2024a Generalised Jeffery's equations for rapidly spinning particles. Part 1. Spheroids. *J. Fluid Mech.* **979**, A1.
- DALWADI, M.P., ISHIMOTO, K., MOREAU, C., GAFFNEY, E.A. & WALKER, B.J. 2024b Generalised Jeffery's equations for rapidly spinning particles. Part 2. Helicoidal objects with chirality. J. Fluid Mech. 979, A2.
- DERR, N.J., DOMBROWSKI, T., RYCROFT, C.H. & KLOTSA, D. 2022 Reciprocal swimming at intermediate Reynolds number. *J. Fluid Mech.* **952**, A8.
- DEY, R., BUNESS, C.M., HOKMABAD, B.V., JIN, C. & MAASS, C.C. 2022 Oscillatory rheotaxis of artificial swimmers in microchannels. *Nat. Commun.* 13 (1), 2952.
- DIAZ, K., ROBINSON, T.L., AYDIN, Y.O., AYDIN, E., GOLDMAN, D.I. & WAN, K.Y. 2021 A minimal robophysical model of quadriflagellate self-propulsion. *Bioinspir. Biomim.* 16 (6), 066001.
- DILUZIO, W.R., TURNER, L., MAYER, M., GARSTECKI, P., WEIBEL, D.B., BERG, H.C. & WHITESIDES, G.M. 2005 Escherichia coli swim on the right-hand side. *Nature* 435 (7046), 1271–1274.
- ELGETI, J., WINKLER, R.G. & GOMPPER, G. 2015 Physics of microswimmers—single particle motion and collective behavior: a review. *Rep. Prog. Phys.* **78** (5), 056601.
- EZHILAN, B., SHELLEY, M.J. & SAINTILLAN, D. 2013 Instabilities and nonlinear dynamics of concentrated active suspensions. *Phys. Fluids* **25** (7), 070607.
- FRIES, J., EINARSSON, J. & MEHLIG, B. 2017 Angular dynamics of small crystals in viscous flow. *Phys. Rev. Fluids* 2 (1), 014302.
- GAFFNEY, E.A., DALWADI, M.P., MOREAU, C., ISHIMOTO, K. & WALKER, B.J. 2022a Canonical orbits for rapidly deforming planar microswimmers in shear flow. *Phys. Rev. Fluids* 7 (2), 1–8.
- GAFFNEY, E.A., DALWADI, M.P., MOREAU, C., ISHIMOTO, K. & WALKER, B.J. 2022b Canonical orbits for rapidly deforming planar microswimmers in shear flow. *Phys. Rev. Fluids* 7 (2), L022101.
- GAFFNEY, E.A., GADÊLHA, H., SMITH, D.J., BLAKE, J.R. & KIRKMAN-BROWN, J.C. 2011 Mammalian sperm motility: observation and theory. *Annu. Rev. Fluid Mech.* 43 (1), 501–528.
- GOLDSTEIN, R.E. 2015 Green algae as model organisms for biological fluid dynamics. *Annu. Rev. Fluid Mech.* 47 (2015), 343–375.
- GORDON, R., LOSIC, D., TIFFANY, M.A., NAGY, S.S. & STERRENBURG, F.A.S. 2009 The Glass Menagerie: diatoms for novel applications in nanotechnology. *Trends Biotechnol.* 27 (2), 116–127.
- HILL, J., KALKANCI, O., MCMURRY, J.L. & KOSER, H. 2007 Hydrodynamic surface interactions enable Escherichia coli to seek efficient routes to swim upstream. *Phys. Rev. Lett.* 98, 068101.
- HOPE, A., CROZE, O.A., POON, W.C.K., BEES, M.A. & HAW, M.D. 2016a Resonant alignment of microswimmer trajectories in oscillatory shear flows. *Phys. Rev. Fluids* 1 (5), 051201.
- HOPE, A., CROZE, O.A., POON, W.C.K., BEES, M.A. & HAW, M.D. 2016b Resonant alignment of microswimmer trajectories in oscillatory shear flows. *Phys. Rev. Fluids* 1, 051201.
- HUANG, H.-W., SAKAR, M.S., PETRUSKA, A.J., PANE, S. & NELSON, B.J. 2016 Soft micromachines with programmable motility and morphology. *Nat. Commun.* 7, 12263.
- IACOVACCI, V., DILLER, E., AHMED, D. & MENCIASSI, A. 2024 Medical microrobots. Annu. Rev. Biomed. Engng 26, 561–591.
- ISHIKAWA, T. 2024 Fluid dynamics of squirmers and ciliated microorganisms. *Annu. Rev. Fluid Mech.* **56** (1), 119–145.
- ISHIKAWA, T., MORITA, T. & OMORI, T. 2022 Soft microswimmer powered by fluid oscillation. *J. Robot. Mech.* **34** (2), 298–300.
- ISHIMOTO, K. 2017 Guidance of microswimmers by wall and flow: thigmotaxis and rheotaxis of unsteady squirmers in two and three dimensions. *Phys. Rev. E* **96** (4), 043103.
- ISHIMOTO, K. 2020a Helicoidal particles and swimmers in a flow at low Reynolds number. *J. Fluid Mech.* **892**, A11.
- ISHIMOTO, K. 2020b Jeffery orbits for an object with discrete rotational symmetry. *Phys. Fluids* **32** (8), 081904.
- ISHIMOTO, K. 2023 Jeffery's orbits and microswimmers in flows: a theoretical review. *J. Phys. Soc. Japan* **92** (6), 062001.
- ISHIMOTO, K. & GAFFNEY, E.A. 2014 Swimming efficiency of spherical squirmers: beyond the Lighthill theory. *Phys. Rev. E* **90**, 012704.
- ISHIMOTO, K. & GAFFNEY, E.A. 2015 Fluid flow and sperm guidance: a simulation study of hydrodynamic sperm rheotaxis. *J. R. Soc. Interface* **12** (106), 20150172.

E.A. Gaffney, K. Ishimoto and B.J. Walker

- JEFFERY, G.B. 1922 The motion of ellipsoidal particles immersed in a viscous fluid. *Proc. R. Soc. A: Math. Phys. Engng Sci.* **102** (715), 161–179.
- JO, I., HUANG, Y., ZIMMERMANN, W. & KANSO, E. 2016 Passive swimming in viscous oscillatory flows. Phys. Rev. E 94 (6), 063116.
- JUNOT, G., FIGUEROA-MORALES, N., DARNIGE, T., LINDNER, A., SOTO, R., AURADOU, H. & CLÉMENT, E. 2019 Swimming bacteria in Poiseuille flow: the quest for active Bretherton-Jeffery trajectories. Europhys. Lett. 126 (4), 44003.
- KANTSLER, V., DUNKEL, J., BLAYNEY, M. & GOLDSTEIN, R.E. 2014 Rheotaxis facilitates upstream navigation of mammalian sperm cells. *eLife* 3, e03521.
- KARP-BOSS, L., BOSS, E. & JUMARS, P.A. 2000 Motion of dinoflagellates in a simple shear flow. Limnol. Oceanogr. 45 (7), 1594–1602.
- KIM, S. & KARRILA, S.J. 2005 Microhydrodynamics: Principles and Selected Applications. Butterworth– Heinemann series in chemical engineering. Dover Publications.
- KOLLE, S., DUBIELZIG, S., REESE, S., WEHREND, A., KÖNIG, P. & KUMMER, W. 2009 Ciliary transport, gamete interaction, and effects of the early embryo in the oviduct: ex vivo analyses using a new digital videomicroscopic system in the Cow1. *Biol. Reprod.* 81 (2), 267–274.
- LAUGA, E. 2007 Continuous breakdown of Purcell's scallop theorem with inertia. Phys. Fluids 19, 061703.
- LAUGA, E. 2011 Life around the scallop theorem. Soft Matt. 7, 3060–3065.
- LAUGA, E., DILUZIO, W.R., WHITESIDES, G.M. & STONE, H.A. 2006 Swimming in circles: motion of bacteria near solid boundaries. *Biophys. J.* **90** (2), 400–412.
- LAUGA, E. & POWERS, T.R. 2009 The hydrodynamics of swimming microorganisms. *Rep. Prog. Phys.* 72 (9), 096601.
- MA, K., PUJARA, N. & THIFFEAULT, J.-L. 2022 Reaching for the surface: spheroidal microswimmers in surface gravity waves. *Phys. Rev. Fluids* 7 (1), 014310.
- MATHIJSSEN, A.J.T.M., FIGUEROA-MORALES, N., JUNOT, G., CLEMENT, E., LINDNER, A. & ZOETTL, A. 2019 Oscillatory surface rheotaxis of swimming *E. coli* bacteria. *Nat. Commun.* 10, 3434.
- MIKI, K. & CLAPHAM, D.E. 2013 Rheotaxis guides mammalian sperm. Curr. Biol. 23 (6), 443-452.
- MOREAU, C. & ISHIMOTO, K. 2021 Driving a microswimmer with wall-induced flow. *Micromachines* 12 (9), 1025.
- MORITA, T., OMORI, T. & ISHIKAWA, T. 2018a Biaxial fluid oscillations can propel a microcapsule swimmer in an arbitrary direction. Phys. Rev. E 98 (6), 063102.
- MORITA, T., OMORI, T. & ISHIKAWA, T. 2018b Passive swimming of a microcapsule in vertical fluid oscillation. *Phys. Rev. E* **98** (2), 023108.
- Nelson, B.J., Kaliakatsos, I.K. & Abbott, J.J. 2010 Microrobots for minimally invasive medicine. *Annu. Rev. Biomed. Engng* 12 (2010), 55–85.
- OMORI, T., KIKUCHI, K., SCHMITZ, M., PAVLOVIC, M., CHUANG, C.H. & ISHIKAWA, T. 2022 Rheotaxis and migration of an unsteady microswimmer. *J. Fluid Mech.* 930, 1–17.
- PAK, O.S. & LAUGA, E. 2015 Theoretical models of low-Reynolds-number locomotion. In *Fluid-Structure Interactions in Low-Reynolds-Number Flows* (ed. C. DUPRAT & H. STONE), The Royal Society of Chemistry.
- PURCELL, E.M. 1977 Life at low Reynolds number. Am. J. Phys. 45 (1), 3-11.
- QIU, T., LEE, T.C. & MARK, A. 2014 Swimming by reciprocal motion at low Reynolds number. *Nat. Commun.* 5, 5119.
- RUSCONI, R. & STOCKER, R. 2015 Microbes in flow. Curr. Opin. Microbiol. 25, 1–8.
- SAINTILLAN, D. & SHELLEY, M.J. 2013 Active suspensions and their nonlinear models. C. R. Phys. 14 (6), 497–517.
- SMITH, D.J., GAFFNEY, E.A., GADÊLHA, H., KAPUR, N. & KIRKMAN-BROWN, J.C. 2009 Bend propagation in the flagella of migrating human sperm, and its modulation by viscosity. *Cell Motil. Cytoskel.* **66** (4), 220–236.
- TALBOT, J., ANTOINE, C., CLAUDIN, P., SOMFAI, E. & BÖRZSÖNYI, T. 2024 Exploring noisy Jeffery orbits: A combined Fokker–Planck and Langevin analysis in two and three dimensions. *Phys. Rev. E* 110, 044143.
- THORP, I.S. & LISTER, J.R. 2019 Motion of a non-axisymmetric particle in viscous shear flow. *J. Fluid Mech.* **872**, 532–559.
- USPAL, W.E., POPESCU, M.N., DIETRICH, S. & TASINKEVYCH, M. 2015 Rheotaxis of spherical active particles near a planar wall. *Soft Matt.* 11 (33), 6613–6632.
- VENTRELLA, F.M., PUJARA, N., BOFFETTA, G., CENCINI, M., THIFFEAULT, J.-L. & DE LILLO, F. 2023 Microswimmer trapping in surface waves with shear. *Proc. R. Soc. A: Math. Phys. Engng Sci.* 479 (2278), 20230280.

- WALKER, B.J., ISHIMOTO, K. & GAFFNEY, E.A. 2023 Systematic parameterizations of minimal models of microswimming. Phys. Rev. Fluids 8, 034102.
- WALKER, B.J., ISHIMOTO, K., GAFFNEY, E.A., MOREAU, C. & DALWADI, M.P. 2021 The effects of rapid yawing on simple swimmer models and planar Jeffery's orbits. arXiv:2110.12888.
- WALKER, B.J., ISHIMOTO, K., GAFFNEY, E.A., MOREAU, C. & DALWADI, M.P. 2022a Effects of rapid yawing on simple swimmer models and planar Jeffery's orbits. *Phys. Rev. Fluids* 7 (2), 023101.
- WALKER, B.J., ISHIMOTO, K., MOREAU, C., GAFFNEY, E.A. & DALWADI, M.P. 2022b Emergent rheotaxis of shape-changing swimmers in Poiseuille flow. J. Fluid Mech. 944 (R2), 1–11.
- WOOLLEY, D.M. 2003 Motility of spermatozoa at surfaces. Reproduction 126, 259-270.
- ZÖTTL, A. & STARK, H. 2012 Nonlinear dynamics of a microswimmer in Poiseuille flow. Phys. Rev. Lett. 108 (21), 218104.
- ZÖTTL, A. & STARK, H. 2014 Hydrodynamics determines collective motion and phase behavior of active colloids in quasi-two-dimensional confinement. *Phys. Rev. Lett.* 112 (11), 118101.